Swiss J Palaeontol (2015) 134:257–279
DOI 10.1007/s13358-015-0084-z

3-D orientation and distribution of ammonites in a concretion from the Upper Cretaceous Pierre Shale of Montana

Neil H. Landman[1] · Joyce C. Grier[2] · James W. Grier[3] · J. Kirk Cochran[4] · Susan M. Klofak[1]

Received: 27 February 2015 / Accepted: 28 May 2015 / Published online: 22 July 2015

Abstract One of the most common modes of preservation of ammonites in the Upper Cretaceous US Western Interior is in concretions. We examine an accumulation of ammonites from a single concretion in the lower Maastrichtian Pierre Shale of eastern Montana. The concretion is an oblate spheroid 50 cm in length and 26 cm in diameter, with its long axis parallel to the substrate. It contains approximately 90 ammonite specimens representing three species of *Hoploscaphites* including adults and juveniles. The concretion also contains other fauna, primarily bivalves and gastropods. A total of 33 ammonites, mostly adults, are concentrated in a cluster that spans 71 % of the length of the concretion (called the "sculpture"). 3-D measurements of the ammonites in the sculpture reveal that (1) the shells dip at all angles, with a significant trend toward more horizontal from west to east; (2) the shells dip with a highly significant bias toward the east, suggesting a current from that direction; and (3) a highly significant number of the shells that are non-vertical face with their left side up. Most of the shells show lethal damage as indicated by missing pieces of body chamber. After settling to the bottom, the shells may have piled up against each other, creating a sediment trap. Other organisms such as scavenging gastropods may have been attracted to the site to feed on the stranded ammonite carcasses. The chambers of the ammonite phragmocones and even some of the body chambers are empty, suggesting relatively rapid burial. Oxygen and carbon isotopic analyses of the ammonite shells reveal that they preserve their original isotopic signature. The values of $\delta^{13}C$ of the carbonate cement in the concretionary matrix are much lighter than those in the ammonite shells and imply that cementation of the concretion occurred in association with the decomposition of organic matter.

Keywords Ammonites · Cretaceous · Taphonomy · Pierre Shale · Concretion

Introduction

One of the most common modes of preservation of ammonites in the Upper Cretaceous US Western Interior is in concretions (Waage 1964; Kauffman and Caldwell 1993; Tsujita 1995; Tsujita and Westermann 1998; Larson et al. 1997; Landman and Klofak 2012). Because such concretions form early in diagenesis, the ammonites are preserved in three dimensions. In addition to ammonites, concretions commonly contain gastropods, bivalves, crustaceans, and other fauna. In an effort to elucidate the processes governing the accumulation of ammonites on the sea floor and the formation of concretions, we investigated a large, ammonite-rich concretion from the Upper Cretaceous Pierre Shale of Montana. We developed a 3-D framework for recording the position and orientation of the ammonites in the concretion. We also documented the

While this manuscript was in press, Susan M. Klofak passed away on May 15, 2015. We dedicate this manuscript to her memory.

✉ Neil H. Landman
landman@amnh.org

[1] Division of Paleontology (Invertebrates), American Museum of Natural History, Central Park West at 79th Street, New York, NY 10024, USA

[2] 17648 57th Ave N, Hawley, MN 56549, USA

[3] Department of Biological Sciences, North Dakota State University, Fargo, ND 58102, USA

[4] School of Marine and Atmospheric Sciences, Stony Brook University, Stony Brook, NY 11794-5000, USA

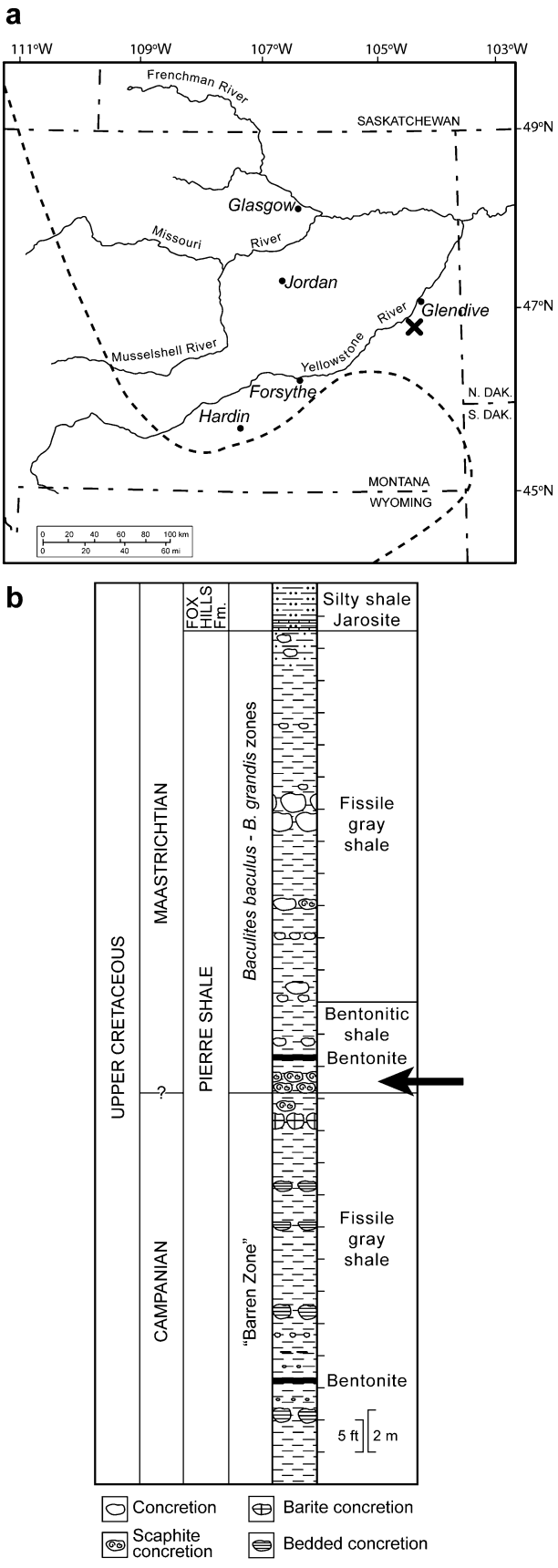

Fig. 1 **a** Map of AMNH loc. 3498 on the Cedar Creek Anticline, Dawson County, Montana. The *dashed line* indicates the shoreline during the time of deposition of the lower Maastrichtian *Baculites baculus* Zone. The Sheridan Delta extends into southeastern Montana (after Reiskind 1975). **b** Stratigraphic section of the study area (after Bishop 1973). The study concretion (*arrow*) occurs below a bentonite at the base of the *B. baculus* Zone

associated fauna and analyzed the oxygen and carbon isotopic composition of the ammonite shells and concretionary matrix.

Geologic setting

The Pierre Shale is a dark gray clayey to silty mudstone that is exposed in large parts of the Northern Great Plains (Gill and Cobban 1966). It is time equivalent to the Bearpaw Shale in northern and western Montana, Alberta, Saskatchewan, and possibly Manitoba (depending on reference, e.g., Bamburak and Nicolas 2009). It is Campanian to Maastrichtian in age. The Pierre Shale was deposited in the Western Interior Seaway, which stretched from the Gulf of Mexico to the Arctic Ocean, and from central Colorado to eastern Kansas. For more information about the nomenclatural history, lithology, stratigraphy, paleontology, and extent of the Pierre Shale, see the original description by Meek and Hayden (1861) plus numerous other references including Kauffman and Caldwell (1993), Cobban et al. (2006), and Martin and Parris (2007).

The study concretion was collected at AMNH locality 3498 near Glendive, Montana, along the Cedar Creek Anticline (Fig. 1a). This area has been described previously by Bishop (1967, 1973), Clement (1986), Grier and Grier (1998), and Grier et al. (1992, 2007). At the time of deposition of the concretion, the shoreline of the Western Interior Seaway was approximately 80 km to the south along the margin of the Sheridan Delta (Reiskind 1975). Recent studies have suggested that most of the Pierre Shale was deposited at a depth of $\leq$100 m (Gill and Cobban 1966; Kauffman and Caldwell 1993; Sageman and Arthur 1994), although the exact water depth is unknown. Palamarczuk and Landman (2011) documented a high incidence of freshwater fungae in slightly older deposits from the Bearpaw Shale of northern Montana, suggesting the possibility of a large embayment in this area open to riverine runoff.

The concretion is one of the "scaphite concretions" described by Bishop (1973), so called because most of the ammonites in the concretion are scaphites. This concretionary scaphite horizon is approximately 1 m below a 7.5 cm-thick bentonite (Fig. 1b). According to Bishop (1973), the base of the scaphite concretions coincides with the base of the lower Maastrichtian *Baculites baculus* Zone. In addition, Walaszczyk et al. (2001) placed the base

of the *Endocostea typica* Zone at approximately 5 m below the base of the scaphite concretions.

We recorded the position of the concretion in the outcrop, noting the ordinal directions. The concretion was oriented with its long axis west to east along a south-facing exposure approximately parallel to the axis of the Cedar Creek Anticline. The long axis of the concretion was parallel to the bedding. It is possible that slumping may have affected the position of the concretion in the outcrop. However, most slumps in the area involve whole blocks of hillside and generally retain the stratigraphic order of the beds. Indeed, two other scaphite concretions were observed at the same stratigraphic horizon as our concretion, approximately 5 and 10 m to the west, suggesting that the stratigraphic sequence was intact.

Methodology

Only a small part of the concretion was initially exposed at the outcrop. The top of it was marked and its position relative to north was recorded. The concretion was broken down into large chunks for transport. Most of the concretion was collected and taken back to the laboratory where it was reassembled like a giant puzzle.

A large 3-D framework with long (610 mm), built-in vernier calipers was designed and constructed (Fig. 2). The reassembled concretion was placed into the framework to measure (1 mm scale) the position and spatial orientation of each ammonite. CT X-ray imaging combined with computerized 3-D reconstruction software is a potential alternative to physically breaking down the concretion. However, the density of ammonite shells is so similar to that of the matrix that attempts so far by us to use CT imaging of ammonites inside concretions have not yielded sufficient resolution of the shells to be practicably useable for our purposes. CT imaging, unless and until the techniques can be further perfected, appears to work best for revealing the internal features that contrast sharply with the concretionary matrix, such as the empty spaces in ammonite phragmocone chambers or worm burrows (cf. Wilson and Brett 2013).

The *X*, *Y*, and *Z* coordinates (1 mm scale) of the surfaces of the chunks and ammonites were recorded, and then each chunk was removed to reveal the next chunk, which was then measured in turn. Each step of the process was photographed with a fixed camera mounted above the frame. After the coordinates of the chunks and ammonites were recorded, the ammonites were exposed using standard preparation techniques with pneumatic tools. Rather than completely separating the ammonites from each other, however, sufficient matrix was left in place to hold various ammonites together in their original position relative to each other so that 33 of the ammonites could then be reassembled into a single structure (hereafter, referred to as the "sculpture") with all the components in their original position. We then remeasured the *X*, *Y*, and *Z* coordinates of the ammonites exposed in the sculpture. The sculpture features the largest and most complete ammonite specimens in the concretion, although smaller and less complete individuals also occur in the surrounding matrix and were subsequently removed.

After the sculpture was prepared, it and the other parts of the concretion were weighed and their volume was determined by water displacement. Most of the smaller pieces were measured together in groups and the larger pieces measured individually. The weights and volumes were measured in grams and milliliters, respectively. The density was calculated from the mass and volume. Weights were measured on a digital scale with a range of 0–25,000 g. All specimens were weighed dry. Volume was measured by water displacement in containers appropriate for the size of the sample.

The terms used to describe the morphology of scaphitid ammonites (hereafter called scaphites) in the concretion are borrowed from Landman et al. (2010, 2012). The adult scaphite shell consists of two parts: a closely coiled phragmocone and a slightly to strongly uncoiled body chamber. The part of the phragmocone that is exposed in the adult shell (as compared to the part that is concealed inside) is called the adult phragmocone. The body chamber consists of the shaft, beginning near the last septum, and a hook terminating at the aperture. The point at which the hook curves backward is called the point of recurvature. Scaphites occur as dimorphs, which are referred to as macroconchs (*M*) and microconchs (*m*). They are interpreted as sexual in nature, the macroconch being the female and the microconch being the male (Cobban 1969; Davis et al. 1996).

The dip angle of the median plane of each complete or nearly complete ammonite in the sculpture was measured, ranging from 0° for a horizontal shell to 90° for a vertical shell. The angle was measured in 5° increments by holding a thin wooden rod parallel to the midline of the venter to mark the median plane, and then holding a protractor next to the rod. The compass direction of dip was measured as an arrow pointing downward from the highest to lowest point of the shell at an angle from 0 to 360° in 5° increments, as viewed from above, with reference to north (0°). We noted which side, left or right, of the ammonite was facing up. The topmost surface of the shell (e.g., aperture, phragmocone, or shaft) was also recorded.

Most, although not all, of the remainder of the concretion was further broken down into small pieces and carefully examined for fauna. The fauna is listed in Table 1 with the authors' names for the species. A few chunks were left intact as positional markers. In recording the number of

Fig. 2 The large 3-D framework with long (610 mm) built-in vernier calipers designed to measure the orientation and position of the ammonites in the concretion. The main accumulation of ammonites (the "sculpture") is visible in the foreground. The view is toward the southeast end of the sculpture and slightly above. The 3-D system is mounted on a wooden frame and consists of two calipers that have had their normal jaws removed from the vernier sliding bars. The rail or ruler of the second, movable one (*Y* axis or width, at the *top* of the photo from *left* to *right*) is attached (with drilled and tapped screws) to the sliding bar of the first, fixed one (*X* axis, or length, at the *left side* of the photo). The end of the second rail rests and slides on top of the wooden bar to the right as the two sliding bars are moved into a particular *X*, *Y* position. A hole was drilled through the sliding part of the second one for a brass rod that can be raised and lowered (*Z* axis, or height). *X* and *Y* are read from the metric scales on their respective rulers. *Z* is read at the top of the brass rod (above and out of the photo) using a metric ruler held alongside the rod. The *bottom end* of the rod is placed at the point to be measured, with the example shown at the umbilicus of AMNH 85455, a specimen of *Hoploscaphites crassus*

species and specimens, we did not normalize for differences in the amount of matrix examined. The position of the fossils in the concretion was recorded according to the chunks in which they occurred. We then grouped the chunks into western and eastern halves, and upper, middle, and bottom thirds of the concretion. The following categories were used in the sampling of each species—uncommon: 1–5 specimens; common: 6–20 specimens; abundant: 21–30 specimens; very abundant: >30 specimens. The microstructure of the outer shell wall of several ammonites was examined under SEM to determine the state of preservation, following the preservation index (PI) of nacre developed by Cochran et al. (2010).

We analyzed several samples for oxygen and carbon isotopic composition. We selected samples from the outer shell wall of the ammonites, calcite from inside the phragmocone chambers, concretionary matrix, and crystalline material in the fractures of the concretion. Several samples were analyzed by X-ray crystallography to determine mineralogy. Samples were selected to represent different regions of the concretion (top, bottom, ends, center) and then assigned random numbers for the purpose of insuring objective, blind measurements. Similarly, we included replicate samples to assess consistency of measurements. Before isotopic analyses, we cleaned the shell material under a light microscope to remove any adhering particles from the surface and subsequently rinsed it in distilled water.

Isotopic analyses were performed at the Keck Paleoenvironmental and Environmental Stable Isotope Laboratory (KPESIL) at the University of Kansas. Samples were reacted with phosphoric acid to release CO_2, which was then analyzed for C and O isotopes using a Thermo Finnigan dual inlet MAT253 isotope ratio mass spectrometer (IRMS). Three standards were used—NIST (National Institute of Standards) NBS-18, NBS-19, and an internally calibrated calcite standard—which were included with each run to generate a three-point calibration curve to the VPDB scale. A fourth standard, NIST 88b dolomitic limestone, acted as a quality control. The percent weight carbonate of the concretionary matrix was also determined by dissolving a sample of matrix with no apparent shell material in HCl.

All specimens are reposited at the American Museum of Natural History, New York, New York (AMNH). They bear as many as four numbers: AMNH specimen number (5

Table 1 List of fauna in the concretion (alphabetical within larger grouping)

Species	Habitat	Feeding strategy	Abundance
Cephalopoda			
Baculites sp. cf. *B. baculus* (Meek and Hayden 1861)	Nektonic	Planktivore	Uncommon
Hoploscaphites crassus (Coryell and Salmon 1934)	Nektonic	Planktivore	Very abundant
Hoploscaphites plenus (Meek 1876)	Nektonic	Planktivore	Very abundant
Hoploscaphites saltgrassensis (Elias 1933)	Nektonic	Planktivore	Abundant
Coleoid	Nektonic	Carnivore	Uncommon
Bivalvia			
Anomia gryphorhyncha (Meek 1872)	Epifaunal	Sessile suspension feeder	Uncommon
Crenella elegantula (Meek and Hayden 1861)	Epifaunal	Mobile deposit feeder	Uncommon
Cucullaea nebrascensis (Owen 1852)	Infaunal	Mobile suspension feeder	Common
Cuspidaria moreauensis (Meek and Hayden 1856a)	Infaunal	Burrowing carnivore	Common
Cuspidaria ventricosa (Meek and Hayden, 1856a)	Infaunal	Burrowing carnivore	Common
Cymbophora warrenana (Meek and Hayden 1856b)	Infaunal	Mobile suspension feeder	Uncommon
Endocostea typica Whitfield, 1877	Epifaunal	Suspension feeder	Common
Limopsis striatopunctata (Evans and Shumard 1857)	Epifaunal	Mobile suspension feeder	Uncommon
Malletia evansi (Meek and Hayden 1856a)	Infaunal	Mobile deposit feeder	Common
Modiolus galpinianus (Evans and Shumard 1854)	Semi-infaunal	Suspension feeder	Uncommon
Modiolus meeki (Evans and Shumard 1857)	Semi-infaunal	Suspension feeder	Common
Nucula cancellata Meek and Hayden, 1856a	Infaunal	Mobile deposit feeder	Very abundant
Nucula percrassa (Conrad 1858)	Infaunal	Mobile deposit feeder	Common
Nucula planomarginata (Meek and Hayden 1856a)	Infaunal	Mobile deposit feeder	Common
Nuculana (*Jupiteria*) *scitula* (Meek and Hayden 1856a)	Infaunal	Mobile deposit feeder	Common
Nuculana (*Nuculana*) *grandensis* (Speden 1970)	Infaunal	Mobile deposit feeder	Uncommon
Nymphalucina occidentalis (Morton 1842)	Infaunal	Siphonate suspension feeder/ Chemosymbiotic	Abundant
Oxytoma (Hypoxytoma) nebrascana (Evans and Shumard 1857)	Epifaunal	Suspension feeder	Common
Pecten (*Chlamys*) *nebrascensis* (Meek and Hayden 1856a)	Epifaunal	Mobile suspension feeder	Abundant
Phelopteria linguiformis (Evans and Shumard 1854)	Epifaunal	Epibyssate suspension feeder	Uncommon
Pholadomya deweyensis (Speden 1970)	Deep infaunal	Mobile suspension feeder	Uncommon
Protocardia subquadrata (Evans and Shumard 1857)	Infaunal	Mobile deposit feeder	Very abundant
Solemya subplicata (Meek and Hayden 1856a)	Infaunal	Siphonate suspension feeder	Uncommon
Tenuipteria fibrosa (Meek and Hayden 1856a)	Epifaunal	Epibyssate suspension feeder	Uncommon
Yoldia rectangularis (Speden 1970)	Infaunal	Mobile suspension feeder	Uncommon
Gastropoda			
Aporrhais biangulata (Meek and Hayden 1856a)	Semi-infaunal	Detritivore	Common
Atira? nebrascensis (Meek and Hayden 1856a)	Epifaunal	Grazer	Very abundant
Cylindrotruncatum demersum (Sohl 1964)	Epifaunal	Carnivore	Common
Drepanochilus evansi (Cossmann 1904)	Epifaunal	Carnivore	Very abundant
Euspira obliquata (Hall and Meek 1856)	Epifaunal	Carnivore	Abundant
Oligoptycha concinna (Hall and Meek 1856)	Epifaunal	Carnivore	Common
Pyrifusus subdensatus (Conrad 1858)	Epifaunal	Carnivore	Uncommon
Rhombopsis intertextus (Meek and Hayden 1856a)	Epifaunal	Carnivore	Uncommon
Scaphopoda			
Dentalium gracile (Hall and Meek 1876)	Semi-infaunal	Carnivore	Very abundant
Dentalium pauperculum (Meek and Hayden 1860)	Semi-infaunal	Carnivore	Very abundant
Coelenterata			
Microbacia radiata (Baron-Szabo 2008)	Epifaunal	Suspension feeder	Uncommon

Table 1 continued

Species	Habitat	Feeding strategy	Abundance
Miscellaneous			
Burrows			Uncommon
Bryozoans	Epifaunal	Suspension feeder	Uncommon
Circular fossils			Uncommon
Crustaceans	Epifaunal	Carnivore	Uncommon
Echinoids	Epifaunal	Carnivore	Common
Epibionts			Uncommon
Fish	Nektonic	Carnivore	Abundant
Ghost rings			Uncommon
"Seeds"			Uncommon
Tubes			Uncommon
Wood/bone			Uncommon

digits, e.g., 36654), study number (1 to 3 digits, e.g., 122), chunk number (number and letter, e.g., 8A-1), and isotopic sample number (letters and number, e.g., OS-7).

Results

Sedimentology of the concretion

The concretion is an oblate spheroid 50 cm in length and 26 cm in diameter, with its long axis parallel to the substrate. The mass of the concretion is 39.5 kg and the volume is 15.0 l; the density of the concretion is 2.63, similar to that of calcite. The concretion consists of finely bioturbated, dark gray, silty mudstone without any indication of primary sedimentary structures. It is 77.4 % calcium carbonate by weight. After dissolution of a sample of the concretionary matrix using HCl, the remaining material is a silty mud.

The crystals inside the chambers of the ammonite phragmocones are composed of calcite. In addition, the concretion contains many fracture planes that are covered with flat, brown, coarsely crystalline calcite, with a maximum thickness of 1 mm (for example, VC 81 and VC 62). Other fracture planes are covered with fibrous yellow calcite (for example, VC 44).

The distribution of fossils in the concretion is uneven, with, for example, clumps of gastropods. The sculpture occupies the central and eastern parts of the concretion. The long axis of the sculpture is coincident with the long axis of the concretion. The sculpture is 35.5 cm long (from one end to the other), 23.5 cm wide, and 13.3 cm thick (Figs. 2, 3, 4). It spans 71 % of the length of the concretion. The ammonites in the sculpture are matrix supported, but mostly in contact with each other. The chambers of most of the ammonites in the sculpture are hollow or filled with calcite crystals, indicating that they were hollow at the time of burial.

Cephalopods

The concretion contains approximately 90 specimens of cephalopods, most of which are scaphites (Table 2; Figs. 2, 3, 4, 5, 6, 7). They comprise three species: *Hoploscaphites crassus*, *H. plenus*, and *H. saltgrassensis*. The majority of these specimens are adults, either broken or whole, although smaller specimens are also present. Of the latter, some are clearly broken phragmocones of larger adults, whereas others, such as AMNH 64484, which is 8 mm in diameter, are probably the broken phragmocones of small juveniles (Fig. 5f). Besides scaphites, the only other ammonites are baculites. We observed ten fragments, all of which are body chambers of juveniles. We attribute them to *Baculites baculus* based on the assignment of this part of the stratigraphic section to the *B. baculus* Zone by Bishop (1967). A coleoid gladius and jaw are also present (Figs. 5i, 6b–d).

Most of our observations about the scaphites relate to the large accumulation of specimens forming the sculpture. The shells are iridescent white to yellowish brown in appearance, with no evidence of encrustation by epibionts. The original aragonitic mineralogy and nacreous microstructure are preserved. The microstructure of the ammonite shells exhibits a range of preservation (e.g., Fig. 5e). According to the preservation index developed by Cochran et al. (2010), the PI ranges from 1.5 to 4.0. In many of the specimens, the phragmocone is hollow or filled with calcite crystals, but not matrix.

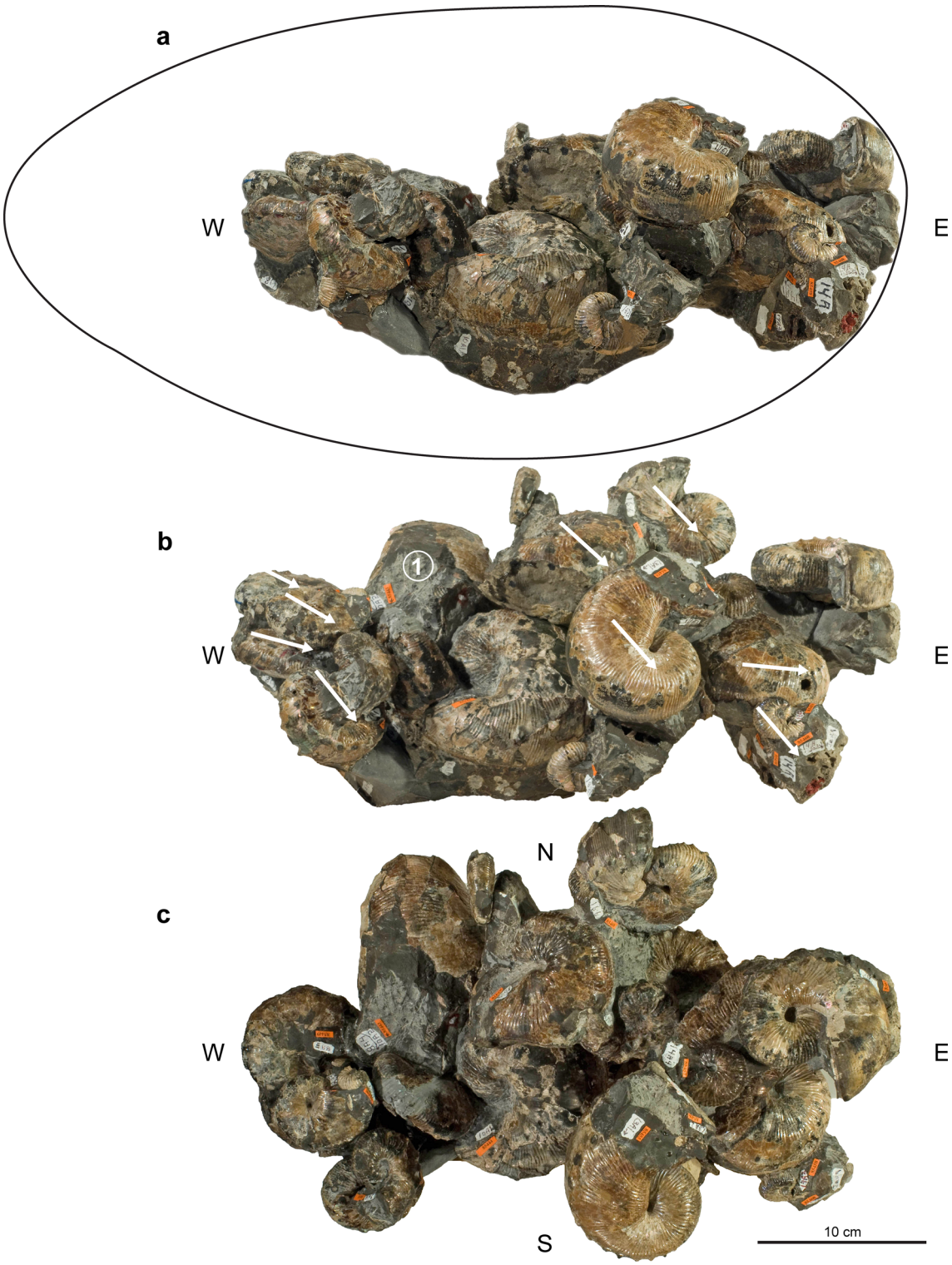

Fig. 3 "Sculpture" of ammonites in the east-central part of the concretion shown in three views, side from south (**a**), high oblique from south (**b**), and top (**c**). The side view includes an outline of the concretion relative to the sculpture. The *arrows* in the high oblique view indicate the angle and direction of dip of the ammonites. The specimen marked "1" is thought to be the first ammonite to have settled on the bottom

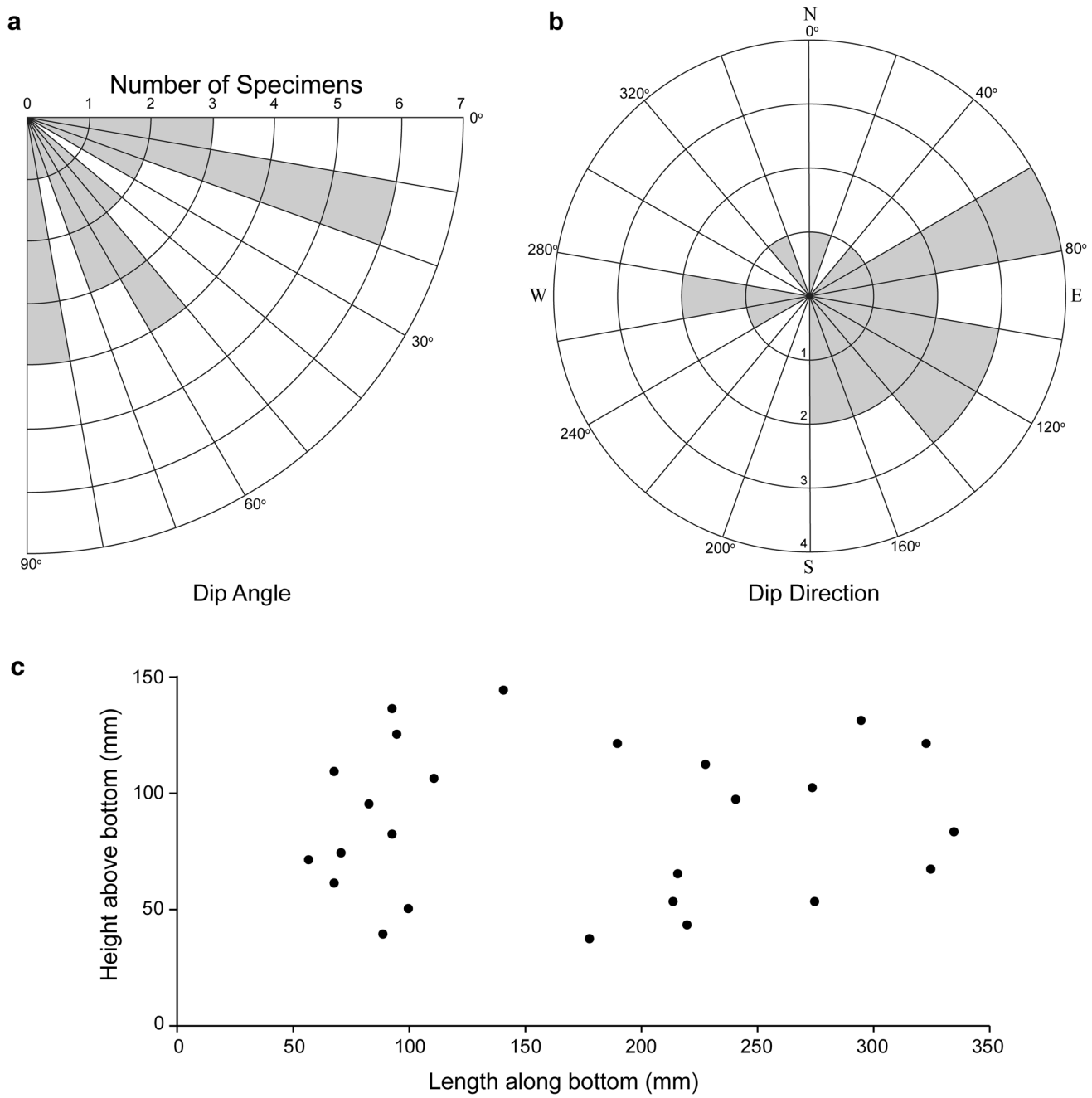

Fig. 4 **a** Dip angle of the ammonites in the sculpture (0° = horizontal, 90° = vertical). **b** Dip direction of the ammonites in the sculpture (0° = north). Most of the ammonites dip preferentially toward the east. **c** Plot of the lowest points of the ammonites in the sculpture with respect to their height and length along the bottom

Of the 29 specimens in the sculpture in which the species can be identified, 16 are *Hoploscaphites crassus*, 8 are *H. saltgrassensis*, and 5 are *H. plenus* (Figs. 3, 5). Most of these specimens are adults. Of the 20 specimens in which the dimorph can be identified, 9 are macroconchs and 11 are microconchs. Most of the specimens are incomplete. The sizes of the specimens are listed in Table 2. The largest, most complete specimen is a macroconch of *H. crassus*, 113 mm in length.

The ammonites in the sculpture dip at almost all angles from 0° (horizontal) to 90° (vertical) (Table 3; Fig. 4a). However, a significant trend exists with dip angles becoming less vertical and more horizontal from west to east (regression of dip angle on west–east distance based

Table 2 Description of ammonites in the "sculpture"

Study no.	AMNH no.	Species	Size (mm)	M/m	Description	Predation	Location of damage	Hollow phrag?
7A1	85445	*crassus*	58.3	m	Incomplete adult	?	Phrag + apt	Yes
7D1	85454	*crassus*	54.7	m	Incomplete adult	Yes	Puncture in phrag + apt	
8A1	85450	*crassus*	97.9	M	Incomplete adult	Yes	Venter of shaft	Yes
8A2	85453	*salt*	78.0	M	Incomplete adult	?	Apt	?
8A3	85447	*salt*	53.9	M	Incomplete adult	Yes	Adoral bc	No
8A4/10A	85443	*salt*	64.9	M	Incomplete adult	?	Adoral bc	No
8A5	85449	*salt*	69.0	M	Incomplete adult	Yes	Adap bc + phrag	No
8A6	85446	*crassus*	58.0	m	Incomplete adult	Yes	Missing adoral bc	No
8A7	85452	*salt*	47.8	m	Incomplete adult	Yes	Adap bc	No
8A8	85451	*plenus*	41.0	?	Incomplete adult	Yes	bc	No
8A9	85448	?	16.8	?	Piece of phrag (juv?)	–	–	Yes
10A1	85444	*crassus*	104.5		Incomplete adult	Yes	Adap bc + apt	No
12B1	85482	*plenus*	23.3	?	Piece of bc (adult?)	?	bc	–
12C1	85481	*plenus*	42.7	?	Incomplete adult	Yes	bc	No
12C2	85483	*crassus*	12.6	?	Piece of phrag	?	Isolated piece	Yes
12C3	85479	*crassus*?	48.8	?	Incomplete adult	Yes	Along side	Yes
12D1	85480	*salt*	36.4	m	Incomplete adult	?	Apt	Yes
13A1	85455	*crassus*	107.0	M	Incomplete adult	Yes	Venter of bc	No
13A2	85456	?	17.5	–	Juvenile (broken in prep)		–	Yes
14A1	85461	*crassus*	113.0	M	Nearly complete adult	Yes	Venter of shaft	Yes
14A2	85458	*salt*	27.0	m?	Incomplete adult	Yes	Adap bc	Yes
14A4	85457	*crassus*	32.3	m	Incomplete adult	Yes	bc	No
14A5	85467	*crassus*	80.0	m	Complete adult	–	–	No
14A7	85468	?	11.7	?	Small part of phrag	?	?	No
16-1	85465	*crassus*	66.6	m	Incomplete adult	Yes	Side near apt	?
16-2	85463	*crassus*	54.5	m	Complete adult	–	–	No
16-3	85470	*crassus*	87.9	M	Incomplete adult	Yes	Phrag + adoral part of bc	No
16-4	85471	*salt*	41.1	m	Complete adult			No
16-5	85473	*plenus*	75.2	M	Incomplete adult	Yes	Venter of bc	Yes
16-6	85469	?	22.0	?	Small fragment of bc (juv?)	?	bc	–
16-7	85472	*crassus*	62.0	m	Incomplete adult	Yes	Part of phrag + both ends of bc	–
16-8	–	*crassus*	21.0 (exposed part)	?	Incomplete adult	Yes	Piece of bc	–
16-9	85464	*plenus*	35.0	?	Incomplete adult	?	Phrag + bc	–

plenus = *Hoploscaphites plenus*, *crassus* = *H. crassus*, salt = *H. saltgrassensis*, adap = adapical, apt = aperture, bc = body chamber, juv = juvenile, phrag = phragmocone, prep = preparation, *M* = macroconch, *m* = microconch

on the lowest point of each ammonite, $n = 25$, $F = 4.37$, $P < 0.05$). A total of 5 out of 25 specimens are vertical or nearly vertical. The lowest points of two of these specimens occur on the bottom of the sculpture on the west side (Fig. 4c). One of them (AMNH 85450) extends from the bottom to the top of the sculpture and is inferred to have been the initial specimen in the accumulation (see "Discussion").

The direction of dip of the ammonites in the sculpture shows a highly significant preference toward the east [east vs. west one-way contingency Pearson Chi square = 7.2, $n = 20$ (excluding 2 vertical, 1 horizontal, and 2 pointing straight south), $df = 1$, $P < 0.01$] (Table 3; Fig. 4b). The easterly dip is not related to the position of the ammonite in the sculpture (regression of dip direction vs. position of ammonite along length, west to east, $n = 22$, $F = 1.19$

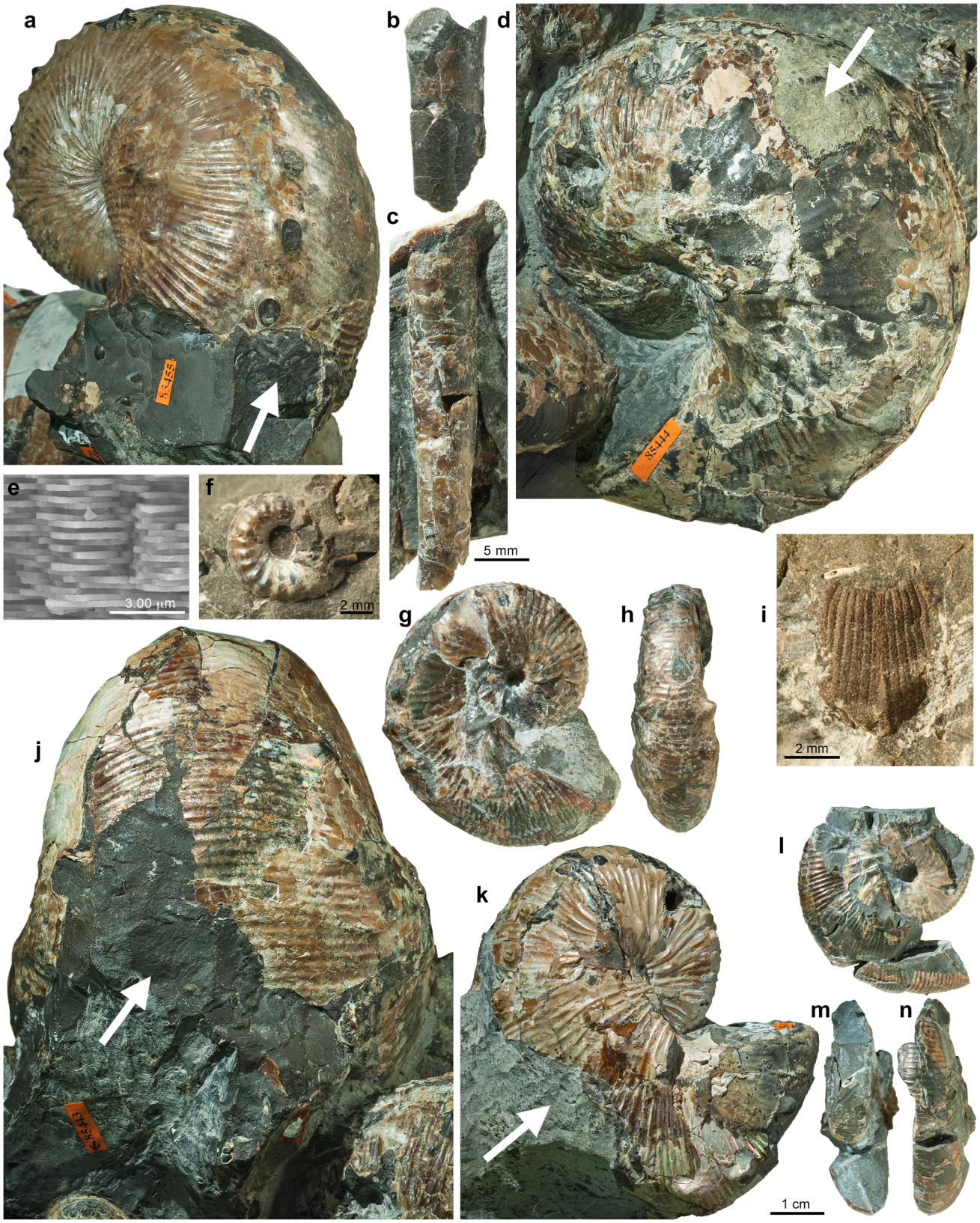
a
b
c
d
e
f
3.00 µm
2 mm
5 mm
g
h
i
2 mm
j
k
l
m
n
1 cm

◀ **Fig. 5** Cephalopods in the concretion. **a** *Hoploscaphites crassus*, macroconch, oblique left lateral view, AMNH 85455, with shell damage on the adoral part of the body chamber (*arrow*). **b**, **c** *Baculites baculus*, juveniles, lateral view. **b** AMNH 64470. **c** AMNH 64442. **d** *H. plenus*, macroconch, oblique left lateral view, AMNH 85444, with large hole in the adapical part of the body chamber (*arrow*). **e** SEM of the microstructure of a sample of the outer shell of *H. crassus*, AMNH 85473, with PI = 3.5. **f** Small, broken phragmocone attributed to *H. crassus* or *H. plenus*, right lateral view, AMNH 64484. **g**, **h** *H. plenus*, microconch, AMNH 63598. **g** Right lateral view. **h** Ventral view. **i** Gladius of an unidentified coleoid, AMNH 63599. **j** *H. crassus*, macroconch, ventral view, AMNH 85450, with large piece of shell missing from the venter of the body chamber (*arrow*). **k** *H. plenus*, macroconch, right lateral view, AMNH 85473, with large chunk of shell missing from the venter of the body chamber (*arrow*). **l–n** *H. saltgrassensis*, microconch, AMNH 64456. **l** Right lateral view. **m** Apertural view. **n** Ventral view

$P > 0.05$). The position of the shells in the sculpture, with respect to the side up, is highly significant (Pearson Chi square = 7.2, $n = 20$, $df = 1$, $P < 0.01$) (Table 3). Most of the shells (16 out of 20) that are not vertical or nearly vertical face left side up. Observations of the highest exposed part of each shell in a sample of 25 specimens in the sculpture reveals the following distribution (Table 3): phragmocone (9), adapical part of the body chamber (5), shaft (5), hook (2), and aperture (4).

Nearly all of the shells in the sculpture are broken (Fig. 5). This damage was probably caused by predation, rather than post-depositional compaction. If it were compaction, all parts of the shell would have been preserved, albeit crushed, whereas the specimens in our sample are not crushed and retain all of the shell except for a missing piece. The missing piece usually occurs at a consistent position at the adapical end of the body chamber. This position is generally interpreted as indicating a lethal injury rather than a random post-depositional break (Takeda et al. 2015). For example, in AMNH 85473, a macroconch of *Hoploscaphites plenus*, a chunk is missing from the right side and venter of the shaft (Fig. 5k), which is undoubtedly due to lethal breakage. Some of the most spectacular examples of lethal breakage are in macroconchs of *H. crassus*. In AMNH 85450, a part of the shell is missing along the venter starting in the shaft and extending to the hook, leaving jagged edges along the margin (Fig. 5j). In AMNH 85444, a hole appears in the adapical end of the body chamber (Fig. 5d). It is 25 mm in diameter with jagged edges. In all of these examples, the animal was probably attacked during life. In AMNH 85455 (13A1), the body chamber is missing on the left and ventral side starting just adapical of the point of recurvature, although part of the aperture is still intact (Fig. 5a). It is possible that this shell was further damaged by scavengers after falling to the sea floor.

In addition to ammonite shells, the concretion contains an estimated 35 cephalopod jaws, most of which are fragments (Fig. 6). All of the jaws are isolated occurrences, outside the body chambers, although none of the whole specimens of ammonites in the sculpture was broken open for inspection. Nearly all of the jaws can be attributed to scaphites. Both upper and lower jaws are present, but lower jaws are more common. The upper jaw consists of a widely open inner lamella and a short reduced outer lamella, both of which converge toward the anterior end. Usually, only the anterior tip of the upper jaw is preserved. The lower jaw is characterized by the presence of a midline slit dividing it into a pair of symmetrical wings. The wings consist of an inner layer of coarsely crystalline black material (originally chitin) and an outer mineralized layer (the aptychus) originally composed of calcite (Kruta et al. 2014). The aptychus is present in at least a few specimens in the concretion, but appears to be recrystallized (Fig. 6i). The chitinous layer is commonly deformed with curled margins.

A few jaws exhibit evidence of predation (Fig. 6). The most spectacular specimen is AMNH 85556 located on the top of the sculpture in chunk 17A (Fig. 6g). It is the right side of a lower jaw 29 mm in maximum length. Based on its size, it probably belongs to *Hoploscaphites crassus*. The posterior of the jaw is torn away along the midline and the middle of the jaw is perforated with a hole with ragged edges. A similarly large lower jaw occurs on the east side of the sculpture (chunk 14A2, AMNH 64552). In addition to ammonite jaws, we observed one coleoid jaw (AMNH 63601). It is an upper jaw characterized by a posteriorly elongate large inner lamella and a short reduced outer lamella (Fig. 6b–d).

Other fauna

In addition to cephalopods, the concretion contains a diverse fauna (38 invertebrate species). The assemblage is dominated by molluscs in terms of number of species and individuals (Table 1; Figs. 7, 8, 9, 10). Most of the bivalve species are infaunal (15 out of 24 bivalve species). The infaunal bivalves are commonly articulated (36 %), either slightly gaping or closed. At least one-half of the infaunal species are nuculids including the genera *Nucula* (3 species) (Fig. 8a–c), *Nuculana* (2 species) (Fig. 8f, g), *Malletia* (1 species) (Fig. 8h), and *Yoldia* (1 species) (Fig. 8i); and the next most abundant infaunal bivalves are *Protocardia subquadrata* (Figs. 8k–m, 9i) and *Nymphalucina occidentalis* (Fig. 9f). Specimens of *P. subquadrata* usually occur in clumps (Fig. 8k). Other common infaunal bivalves are two species of *Cuspidaria*, both of which are carnivores (Fig. 8n, q–s).

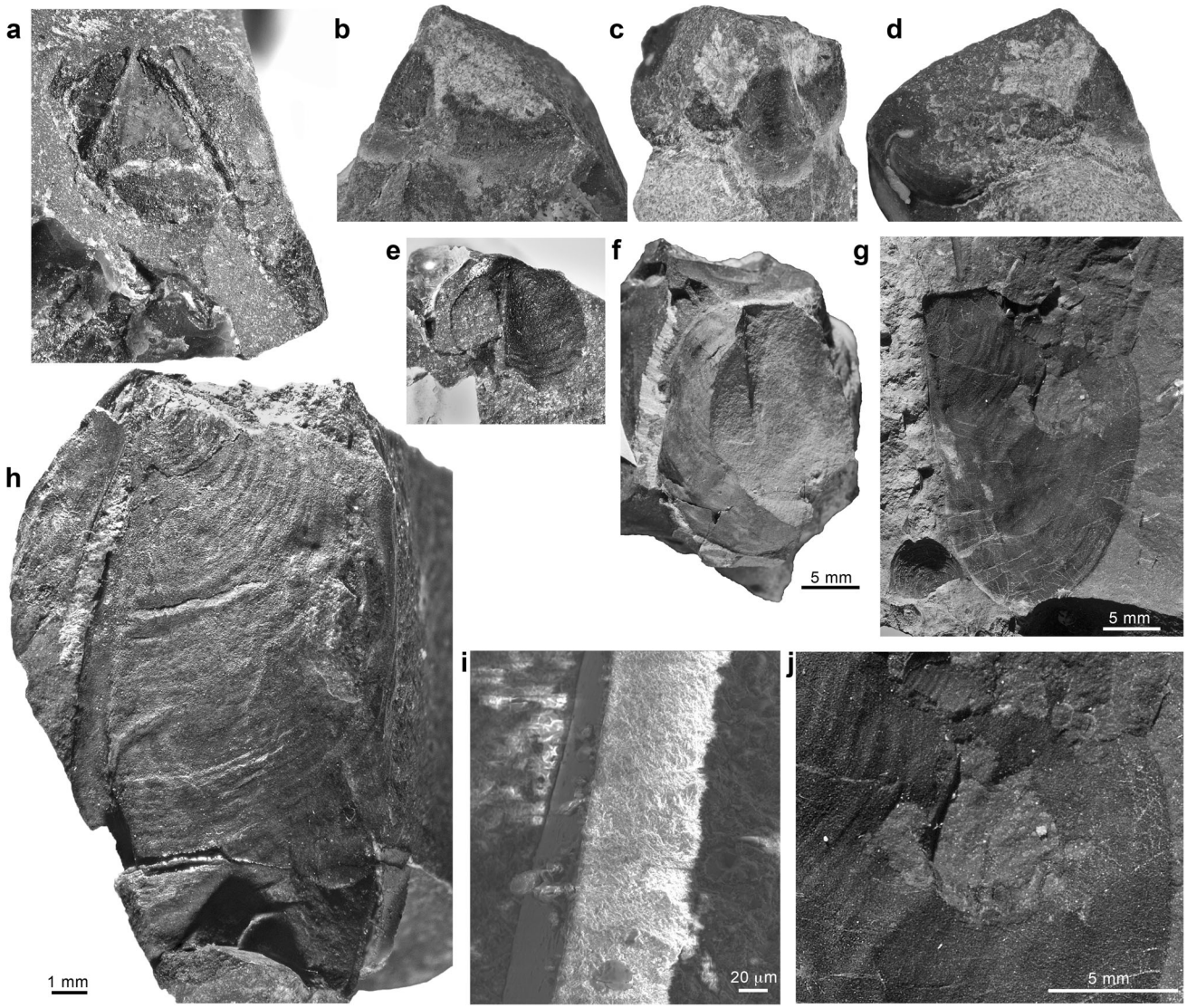

Fig. 6 Cephalopod jaws in the concretion. **a** Tip of an upper jaw attributed to *Hoploscaphites*, dorsal view, AMNH 63600. **b**-**d** Upper jaw of a coleoid, AMNH 63601. **b** Right lateral view. **c** Dorsal view. **d** Left lateral view. **e** Lower jaw attributed to *Hoploscaphites*, dorsal view, AMNH 63602. **f** Lower jaw attributed to *H. crassus*, ventral view, with part of the left side broken off in preparation, AMNH 63603. **g**, **h** Lower jaw attributed to *H. crassus*, AMNH 64498. **g** Right lateral view, with hole produced by predation. **j** Close-up of hole. **h** Lower jaw attributed to *Hoploscaphites*, ventral view, AMNH 63604. **i** SEM of the microstructure of a lower jaw attributed to *Hoploscaphites*, AMNH 64512. The jaw consists of a black layer (*left*) originally composed of chitin, and a mineralized layer called the aptychus (*right*) originally composed of calcite

Epifaunal bivalves comprise 30 % of the bivalve species. They are mostly disarticulated (only 12 % articulated). The most abundant epifaunal bivalve species is *Pecten* (*Chlamys*) *nebrascensis* with 41 specimens (Fig. 9j). The rest of the epifaunal bivalves comprise seven specimens of *Oxytoma* (Fig. 9g), five specimens of pterioids, representing three genera (Fig. 9h, k, l), and a few specimens of *Anomia* (Fig. 9m). The inoceramids are small and incomplete (Fig. 9a). The outer layer of prismatic crystals in the shell of the inoceramids is missing, suggesting that the inoceramids were buried only after the outer layer was lost. The incidence of encrustation on bivalves is low. Some bivalves exhibit circular impressions, which may represent parasites (Fig. 8d). Drill holes are also uncommon, with one in a specimen each of *Protocardia* (Fig. 9i) and *Lucina*.

Gastropods are dominated by carnivores/scavengers in terms of number of species (6 out of 8 species) and number of individuals (approximately 150 out of 200). *Drepanochilus evansi* (Fig. 10a) is the most abundant species, with *Atira? nebrascensis* (not a carnivore, but a grazer) the next most abundant (Fig. 10g, h). The gastropods occur

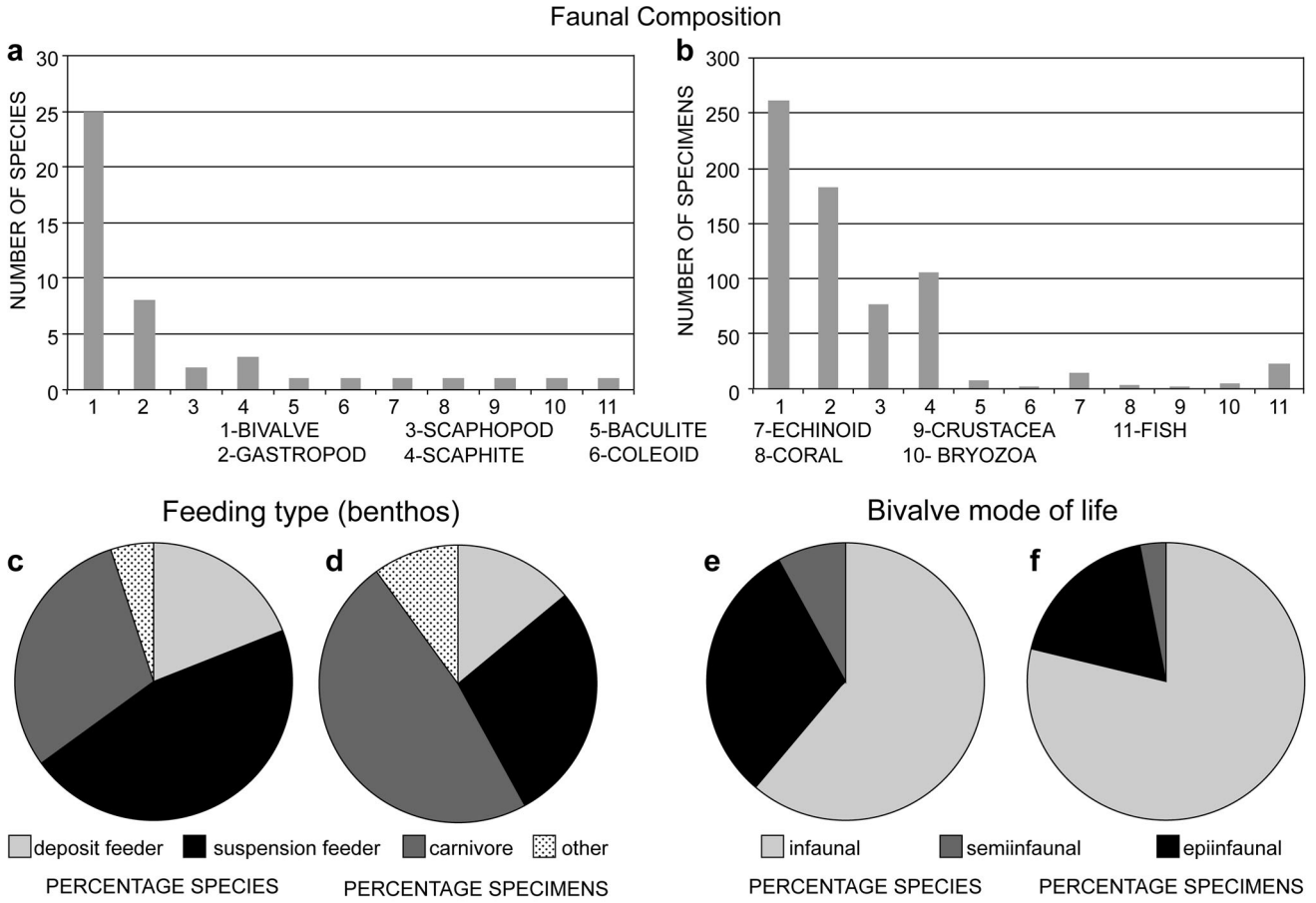

Fig. 7 **a**, **b** Composition of the fauna in the concretion. The fauna is dominated by bivalves and gastropods in terms of both number of species and number of individuals. **c**, **d** Feeding types of the benthos. Suspension feeders dominate in terms of number of species whereas carnivores dominate in terms of number of individuals. **e**, **f** Bivalve mode of life. Infaunal bivalves dominate in terms of both number of species and number of individuals

scattered throughout the concretion, but also occur in small accumulations, for example, clumps of *Drepanochilus* on the west side of the concretion. The incidence of encrustation on gastropods is low.

Of the other fauna, scaphopods are very abundant and comprise two species, *Dentalium gracile* (Fig. 10m–o) and *D. pauperculum* (Fig. 10l), both of which are semi-infaunal carnivores. Several specimens show evidence of healed injuries (Fig. 10m, n) and drill holes (Fig. 10o, p), as described from the Campanian Pierre Shale of Manitoba by Li et al. (2011). Echinoids are also present and are patchy in their distribution (Fig. 9n). Only a few epifaunal suspension feeders including bryozoans and corals are present (Fig. 10e).

With respect to the distribution of fauna in the concretion, the east end of the concretion contains more species and individuals than the west end (38 vs. 32 species, respectively, and 313 vs. 245 individuals, respectively), with a higher abundance of scaphopod specimens on the east end (55 vs. 19, respectively). The top and middle one-third of the concretion each contain nearly the same number of species (35 in the top vs. 33 in the middle), but the number of specimens is higher in the top (369 in the top vs. 194 in the middle). The number of bivalve and gastropod specimens is nearly double in the top compared to the middle (141 vs. 78, respectively, for bivalves, and 121 vs. 45, respectively, for gastropods), with many more epifaunal elements on top (153 vs. 61 specimens, respectively). The top one-third of the concretion also contains the majority of fish bits. In contrast, the bottom one-third of the concretion, especially on the west end, is very depauperate. Few species (17) and individuals (21) are present, including two small juveniles of *Hoploscaphites* (broken phragmocones).

Table 3 Orientation of ammonites in the "sculpture"

Study no.	AMNH no.	Species	Dip angle (°)	Dip direction (°)	Highest point	Side up
7A1	85445	*crassus*	60	110	Phrag	R
7D1	85454	*crassus*	85	265	Shaft	LNV
8A1	85450	*crassus*	85	270	Hook	RNV
8A2	85453	*salt*	20	70	Shaft	L
8A3	85447	*salt*	20	110	Phrag	R
8A4/10A2	85443	*salt*	90	–	Adap bc	V
8A5	85449	*salt*	20	80	Phrag	L
8A6	85446	*crassus*	50	100	Phrag	L
8A7	85452	*salt.*	60	65	Phrag	L
8A8	85451	*plenus*	70	50	Apt	R
8A9	85448	?	60	10	Phrag	L
10A1	85444	*crassus*	30	180	Phrag	L
12C1	85481	*plenus*	90	–	Adap bc	V
13A1	85455	*crassus*	30	130	Shaft	L
14A1	85461	*crassus*	5	70	Shaft	L
14A2	85458	*salt*	65	150	Phrag	R
14A4	85457	*crassus*	12	180	Adap bc	L
14A5	85467	*crassus*	15	330	Apt	L
16-1	85465	*crassus*	10	100	Phrag	L
16-2	85463	*crassus*	50	145	Apt	L
16-3	85470	*crassus*	0	–	Adap bc	L
16-4	85471	*salt.*	75	250	Hook	RNV
16-5	85473	*plenus*	65	135	Apt	L
16-7	85472	*crassus*	60	120	Adap bc	L
16-9	85464	*plenus*	15	135	Shaft	L

plenus = *Hoploscaphites plenus*; *crassus* = *H. crassus*; salt = *H. saltgrassensis*; Adap bc = adapical part of body chamber; Apt = aperture; L = left; LNV = left, but nearly vertical (75°–85°); Phrag = phragmocone; RNV = right, but nearly vertical (75°–85°); R = right; V = vertical

Isotopic analysis

The values of $\delta^{18}O$ and $\delta^{13}C$ of 30 samples from the concretion are reported in Table 4 and shown in Fig. 11. The PIs of the ammonite shells are also listed. The values of $\delta^{18}O$ and $\delta^{13}C$ of the ammonite shells range from −4.01 to −1.25 ‰, and −2.12 to −0.44 ‰, respectively. The values of $\delta^{18}O$ and $\delta^{13}C$ of the chamber calcite range from −1.96 to −0.68 ‰, and −12.63 to −1.73 ‰, respectively. The values of $\delta^{18}O$ and $\delta^{13}C$ of the flat calcite crystals on the fracture planes (VC 62 and VC 81) range from −12.08 to −11.90 ‰, and −25.74 to −25.54 ‰, respectively. The values of $\delta^{18}O$ and $\delta^{13}C$ of the fibrous calcite (VC 44) are −3.49 and −7.01 ‰, respectively. The values of $\delta^{18}O$ and $\delta^{13}C$ of the carbonate cement of the concretionary matrix range from −1.51 to −1.33 ‰, and −15.48 to −9.66 ‰, respectively. The values of $\delta^{18}O$ and $\delta^{13}C$ of the carbonate cement of the crust (outer part) of the concretionary matrix are similar and range from −1.65 to −1.21 ‰, and −17.95 to −17.01 ‰, respectively.

Discussion

Environment of deposition

In the ammonite shells, the values of $\delta^{18}O$ average −2.20 ‰ and range from −4.01 to −1.25 ‰. The average value of the two best-preserved samples (AMNH 85473 and 85484) with PI ≥3 is −2.12 ‰. If the ammonites secreted their shells in isotopic equilibrium with seawater, as in modern nautilus (see Landman et al. 1994), these values reflect the ambient conditions. Using the aragonite-temperature equation of Grossman and Ku (1986), and assuming an average value of $\delta^{18}O$ of Cretaceous sea water of −1.0 ‰ (Shackleton and Kennett 1975; Dennis et al. 2013), the average value of $\delta^{18}O$ of the two best-preserved samples equates to 27.0 °C. This is almost exactly the temperature calculated by Kruta et al. (2014) for the slightly older upper Campanian *Baculites* sp. smooth Zone of the Pierre Shale in South Dakota based on ammonite shells and aptychi.

Three species of scaphites are present in the concretion: *Hoploscaphites crassus*, *H. plenus*, and *H. saltgrassensis*. Nearly all of the specimens are adults, almost evenly divided between macroconchs and microconchs. The predominance of adults in one area may indicate the presence of a breeding ground, but if this hypothesis is correct, it implies that the same breeding ground would have served all three species. It is more likely that the abundance of adults was a response to an ecological event in the area, such as a plankton bloom that attracted the scaphites to prey on the plankton and/or associated animals.

Most of the scaphites show evidence of predation. The damage is significant, involving large parts of the body chamber, and suggests that the jaws of the predators were large enough to accommodate the body chambers of these scaphites, including *Hoploscaphites crassus*, with its very depressed whorl section. Possible predators include sharks, fish, and mosasaurs. Ammonite jaws are also abundant in the concretion and many of them show evidence of predation, such as perforations (see also Landman and Klofak 2012). Thus, the predators must have eaten part or all of the ammonite soft body, possibly regurgitating the jaws afterward, as described by Reboulet and Rard (2008).

After predation, the ammonite shells may have floated for some time in the water column (for a discussion of postmortem drift, see Maeda 1987; Maeda and Seilacher 1996; Tsujita 1995; Tsujita and Westermann 1998; Westermann 1996; Stephen et al. 2012). However, the absence of epibionts on the shells suggests that they soon became waterlogged and settled to the sea floor, perhaps in local depressions. Landman and Cobban (2007) documented a similar sequence of events for scaphites in the Marias River Shale of north-central Montana. As these specimens settled to the bottom, they first touched the sea floor leaving impressions of the venter of the body chamber near the point of recurvature and subsequently fell over.

The ammonites that comprise the sculpture probably did not all settle to the bottom simultaneously. The sequence of deposition can be reconstructed by examining the positions of the ammonites in the sculpture (Figs. 3, 4). The specimens dip preferentially to the east, suggesting a current from that direction. AMNH 85450, a large macroconch of *Hoploscaphites crassus*, is located on the west end of the sculpture (marked number "1" in Fig. 3b). It is vertically oriented and extends from the bottom to the top of the sculpture. It is hypothesized to be the first specimen to have settled on the bottom, with additional specimens piling up against it. The settling of the first few specimens in turn promoted further accumulation of debris by disrupting the current and trapping items on both sides of the obstruction (for further discussion about ammonite accumulations, see Maeda 1987; Maeda and Seilacher 1996).

Most of the shells that are oriented vertically are positioned with the phragmocone and adapical part of the body chamber on top, suggesting the possibility that some ammonites retained relict buoyancy (for a recent discussion of vertically oriented ammonites, see Olivero 2007). Nearly all of the ammonites in the sculpture are oriented with their left side up. This is a highly significant pattern (15 out of 18 specimens). In a few instances (4 specimens), these shells are damaged on the left side, leaving the right side more intact and presumably heavier. But in the rest of the specimens, the damage appears symmetrical, and we are at a loss to explain the left-side up pattern.

The accumulation of ammonites promoted the development of a localized community dominated by bivalves and gastropods. The infaunal bivalves probably lived at the site before, during, and after the deposition of the scaphites. However, the majority of fossils occur in the upper one-third of the concretion, especially the epifaunal bivalves, suggesting that these might have been trapped along with passing sediment due to baffling by the scaphite accumulation. Only 12 % of the epifauna are articulated vs. 36 % of the infauna, implying that the epifuana were either transported in or remained on the seafloor long enough to become disarticulated. The loss of the outer prismatic layer in the inoceramid shells also suggests that they must have suffered disintegration before burial. The large number of carnivorous gastropods implies that they may have been attracted to the site to feed on the scaphite carcasses.

Burial of the ammonite shells and other debris was probably relatively rapid. This is consistent with the fact that most of the chambers of the ammonite phragmocones and even some of the body chambers are empty and free of matrix. The void spaces are covered with calcite crystals. The abundance of jaws in the concretion also indicates relatively rapid burial. No ammonite jaws are visible inside the intact body chambers, but these were not broken open for further inspection. The apical whorls of gastropods are generally filled with calcite, rather than matrix, which also suggests rapid deposition without much sediment resuspension.

Post-depositional history

The isotopic values of the best-preserved ammonite shells record the environment in which the ammonites lived. These values can also be used as a reference point to interpret the diagenetic history of the concretion. The values of $\delta^{13}C$ of the carbonate cement in the concretionary matrix are much lighter than those in the ammonite shells and range from −15.48 to −9.66 ‰. Similarly, the values of $\delta^{13}C$ of the carbonate cement in the crust of the

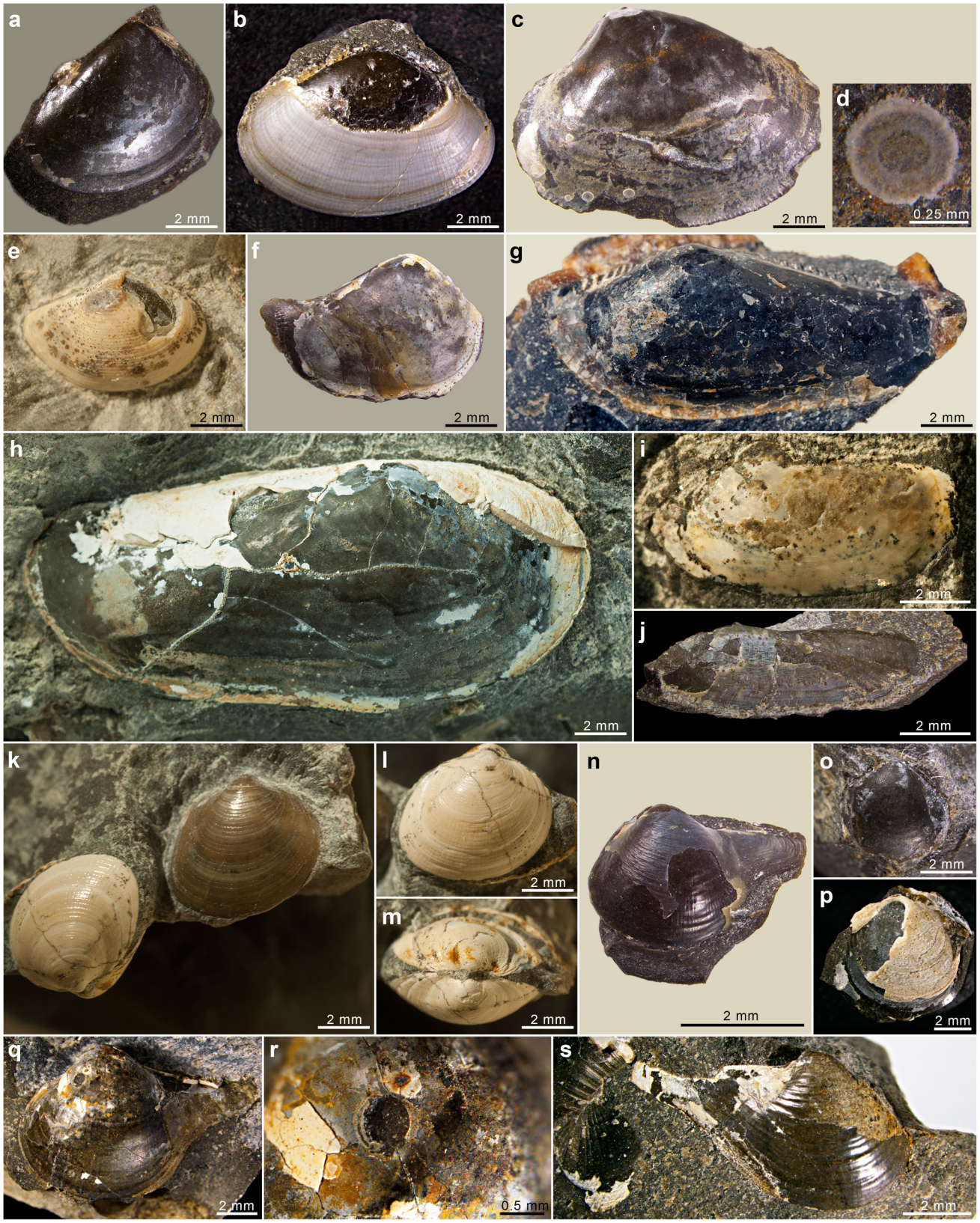
a
2 mm
b
2 mm
c
2 mm
d
0.25 mm
e
2 mm
f
2 mm
g
2 mm
h
2 mm
i
2 mm
j
2 mm
k
2 mm
l
2 mm
m
2 mm
n
2 mm
o
2 mm
p
2 mm
q
2 mm
r
0.5 mm
s
2 mm

◀ **Fig. 8** Bivalves in the concretion. **a** *Nucula planomarginata*, AMNH 63605. **b** *Nucula cancellata*, AMNH 63606. **c** *Nucula percrassa*, with small epibiont, AMNH 63607. **d** Close-up of epibiont in **c**. **e** *Nuculana* (*Jupiteria*) *scitula*, AMNH 63608. **f** *Nuculana* (*Jupiteria*) *scitula*, AMNH 63609. **g** *Nuculana* (*Nuculana*) *grandensis*, AMNH 85570. **h** *Malletia evansi*, AMNH 63610. **i** *Yoldia rectangularis*, AMNH 63611. **j** *Solemya subplicata*, AMNH 63612. **k** *Protocardia subquadrata*, AMNH 63613, 63614. **l**, **m** *Protocardia subquadrata*, AMNH 63614. **n** *Cuspidaria ventricosa*, AMNH 63615. **o** *Cymbophora warrenana*, AMNH 63616. **p** *Cucullaea nebrascensis*, AMNH 63617. **q** *Cuspidaria ventricosa*, with hole, AMNH 63618. **r** Close-up of hole in **q**. **s** *Cuspidaria moreauensis*, AMNH 63619

concretionary matrix are very light and range from −17.95 to −17.01 ‰. These light values probably reflect the decomposition of organic matter, which was undoubtedly associated with the ammonite shells and other faunal debris. The organic matter may also have accumulated on the downcurrent side of the sculpture, promoting the formation of the concretion in this area even though the fossils themselves are not as conspicuous (Fig. 3a, "empty" area in concretion to left of sculpture).

Berner (1968) demonstrated that decomposition of fish tissue in the laboratory results in significant increases in pH, NH_4^+ concentration, and carbonate alkalinity, leading to the precipitation of calcium salts of fatty acids called adipocere. Subsequent conversion of adipocere to calcium carbonate produces a calcium carbonate-cemented concretion with carbonate effectively filling the pore spaces of the sediment. The porosity of muddy sediments in modern soft-bottom settings is relatively high (∼70 % volume). Complete precipitation of $CaCO_3$ in the pore volume of the sediments in our concretion would also have produced a comparable volume of calcium carbonate. Because the density of calcium carbonate is similar to that of terrigenous sediments, the volume of calcium carbonate in the concretion can be estimated by determining the percent mass or weight of calcium carbonate. The weight of calcium carbonate in our concretion, as well as that of the concretion documented by Landman and Klofak (2012), is ∼80 %. Thus, all of the pore volume of the sediments in our concretion was replaced by calcium carbonate.

The values of $\delta^{18}O$ of the carbonate cement in the concretionary matrix are similar to those in the best-preserved shell material. The similarity of these values suggests that cementation occurred under approximately the same environmental conditions as those under which the ammonites secreted their shells. Indeed, most studies suggest that cementation of concretions occurs at shallow burial depths early in diagenesis (Berner 1968; Canfield and Raiswell 1991; Landman and Klofak 2012). The formation of the hard concretion would have prevented the dissolution of the shells and insured their preservation in three dimensions.

The values of $\delta^{18}O$ of the calcite crystals filling the chambers of the ammonites are similar to those of the ammonite shells themselves, suggesting that precipitation of the chamber crystals occurred at approximately the same temperature as that at which the ammonites secreted their shells. Indeed, the crystals may have precipitated from partial dissolution of the aragonitic chamber walls and re-precipitation of calcite inside the closed chambers. However, the values of $\delta^{13}C$ of these crystals are slightly lighter than those of the ammonite shells, possibly reflecting the presence of organic membranes such as thin linings in the chambers. The very light value of a single sample (−12.63 ‰ in 5B-1) can be explained by the fact that this sample is derived from a broken chamber of a phragmocone in contact with the hollow body chamber of the ammonite at the time of burial. It is possible that precipitation of the crystals in this chamber occurred when it was open and exposed to the light carbon fluids involved in the cementation of the concretion.

In contrast to the isotopic composition of the ammonite shells, chamber crystals, and carbonate cement, the isotopic composition of the calcite crystals in the fractures planes is lighter (Fig. 11). The values of $\delta^{18}O$ and $\delta^{13}C$ in the fibrous calcite are −3.49 and −7.01 ‰, respectively, and those in the tabular calcite are even lighter, ranging from −12.08 to −11.90 ‰, and −25.74 to −25.54 ‰, respectively. The fractures may have formed during dewatering and shrinkage of the concretion, and the light values suggest the involvement of groundwater that was depleted in ^{18}O and ^{13}C. The fibrous calcite may have precipitated earlier in the diagenetic history of the concretion and the tabular calcite later, with deeper burial and greater exposure to meteoric water. Carpenter et al. (1988) envisaged a similar scenario in their study of concretions from the Fox Hills Formation of North Dakota.

An alternative explanation for the isotopic composition of the fracture calcite, particularly the tabular crystals, involves precipitation at higher temperatures associated with deeper burial. Dale et al. (2014) used carbonate clumped isotopes to examine the temperature of formation of the carbonate in septarian fractures in concretions from the Mancos Shale. The use of clumped isotopes permitted them to calculate temperatures independent of the isotopic composition of the fluid. Dale et al. (2014) observed values of $\delta^{18}O$ similar to those we observed in the tabular calcite crystals, and calculated temperatures of ∼100 °C, requiring burial of the concretion at a depth of ∼3500 m at the time of septarian carbonate precipitation. These conditions seem unlikely for our concretion and we conclude that meteoric groundwater is a more likely source for the light $\delta^{18}O$ and $\delta^{13}C$ values of the fracture calcite.

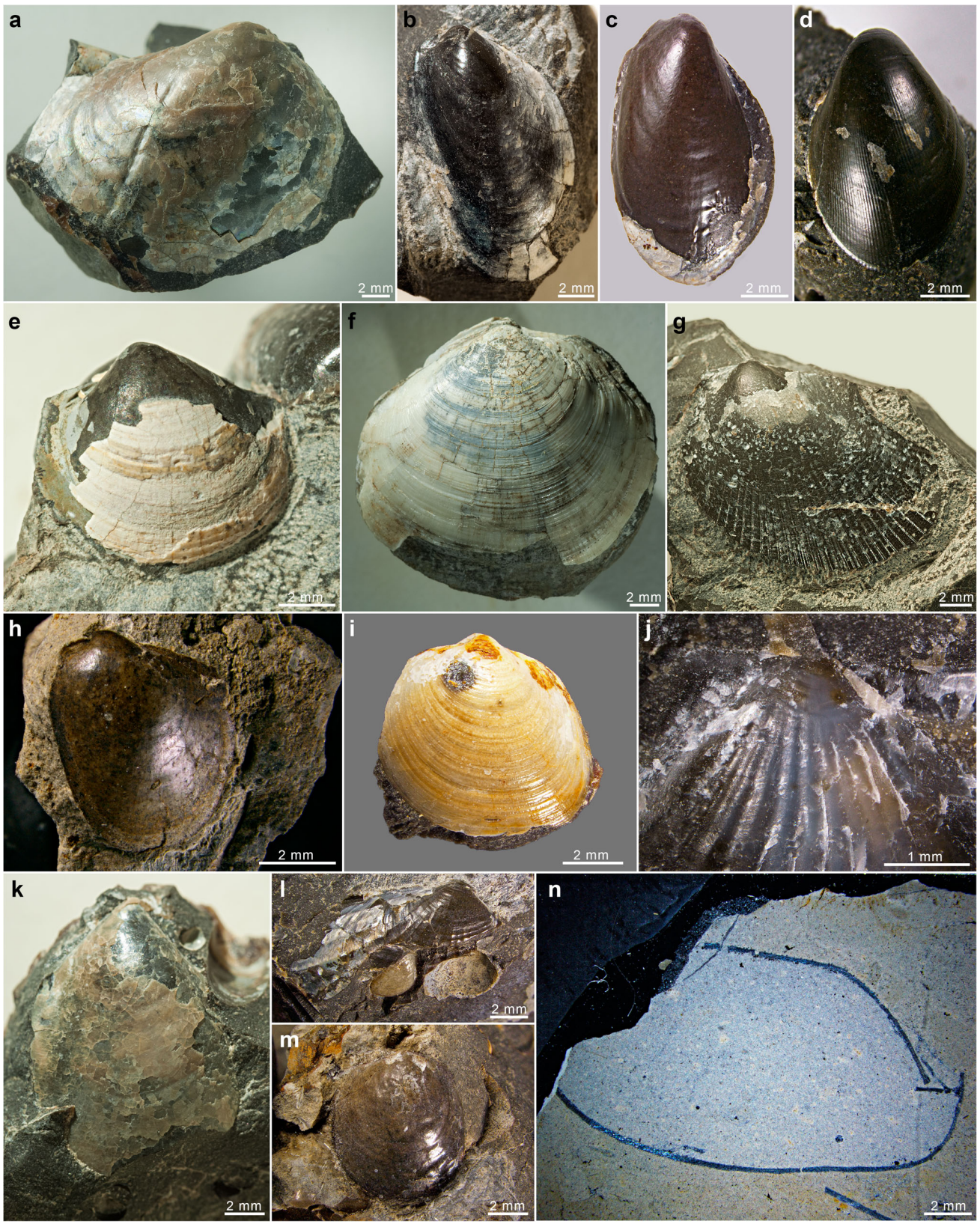
a
2 mm
b
2 mm
c
2 mm
d
2 mm
e
2 mm
f
2 mm
g
2 mm
h
2 mm
i
2 mm
j
1 mm
k
2 mm
l
2 mm
m
2 mm
n
2 mm

◀ **Fig. 9** Bivalves and other fauna in the concretion. **a** *Endocostea typica*, AMNH 63620. **b** *Modiolus meeki*, AMNH 63621. **c** *Modiolus galpinianus*, AMNH 63622. **d** *Crenella elegantula*, AMNH 63623. **e** *Limopsis striatopunctata*, AMNH 63624. **f** *Nymphalucina occidentalis*, AMNH 63625. **g** *Oxytoma* (*Hypoxytoma*) *nebrascana*, AMNH 63626. **h** *Pholadomya deweyensis*, AMNH 63653. **i** *Protocardia subquadrata*, with drill hole, AMNH 63652. **j** *Pecten* (*Chlamys*) *nebrascensis*, AMNH 63651. **k** *Phelopteria linguiformis*, AMNH 63627. **l** *Tenuipteria fibrosa*, AMNH 63628. **m** *Anomia gryphorhyncha*, AMNH 63629. **n** Echinoid in cross-section, AMNH 63630

Summary

The accumulation of fauna in the concretion probably reflects the original site where the initial ammonites settled to the bottom after having been preyed upon. The accumulation of ammonites may have acted as a sediment trap, leading to the deposition of additional debris and sediment over a protracted period of time. In addition, other

Fig. 10 Gastropods and other fauna in the concretion. **a** *Drepanochilus evansi*, AMNH 63631. **b** *Rhombopsis intertextus*, AMNH 63632. **c** *Pyrifusus subdensatus*, AMNH 63633. **d** *Aporrhais biangulata*, AMNH 63634. **e** *Microbacia radiata*, AMNH 63635. **f** Spherule of unknown origin, AMNH 63636. **g** *Atira? nebrascensis*, AMNH 63637. **h** *Atira? nebrascensis*, AMNH 63638. **i** *Euspira obliquata*, AMNH 63639. **j** *Cylindrotruncatum demersum*, AMNH 63640. **k** *Oligoptycha concinna*, AMNH 63641. **l** *Dentalium pauperculum*, AMNH 63642. **m** *Dentalium gracile*, with healed injury, AMNH 63643. **n** Close-up of injury in **m**. **o** *Dentalium gracile*, with hole, AMNH 63644. **p** Close-up of hole in **o**

Table 4 Isotopic analysis of samples in the concretion

Sample type	Sample no.[a]	Lab no.[b]	AMNH no.[c]	PI[d]	Location[e]	$\delta^{18}O$ (‰)	Mean $\delta^{18}O$[f] (‰)	$\delta^{13}C$ (‰)	Mean $\delta^{13}C$[f] (‰)	Comments
OS	1B-1	69	85490	2.5	West end	−1.20	–	−2.06	–	From shell in mold
OS	1B-1[a]	70	85490	2.5	West end	−1.29	−1.25	−1.15	−1.61	As above
OS	14A-1	11	85461	2.0	East end	−1.49	–	−2.20	–	At apt, mid-venter
OS	14A-1[a]	57	85461		East end	−1.27	−1.38	−2.04	−2.12	As above
OS	8A-1	29	85450	2.5	Center	−3.94	–	1.70	–	From apt, mold
OS	8A-1[a]	59	85450		Center	−4.08	−4.01	1.14	1.42	As above
OS	10A-1	36	85444	2.5	Center	−2.35	–	−2.05	–	From apt
OS	10A-1[a]	41	85444	1.5	Center	−2.32	−2.34	0.01	−1.02	Near above but…[g]
OS	16-5	30	85473	3.0	Top	−2.28	–	1.31	–	From shell in mold
OS	16-5[a]	38	85473	3.5	Top	−2.46	−2.37	1.47	1.39	As above
OS	5B-1	14	85484		Low center	−1.70	–	−0.93	–	From phrag, lat
OS	5B-1[a]	58	85484	4.0	Low center	−2.03	−1.86	0.04	−0.44	As above
CC	1B-1	5	85490		West end	−1.23	–	−3.11	–	Last ch, along siph
CC	14A-1	65	85461		East end	−1.80	–	−1.73	–	Near bc, but ch
CC	8A-1	52	85450		Center	−1.28	–	−4.17	–	Near bc, but ch
CC	16-5	10	85473		Top	−2.01	–	−2.87	–	1/3 back from bc
CC	16-5[a]	32	85473		Top	−1.90	−1.96	−2.46	−2.67	As above
CC	5B-1	68	85484		Low center	−0.68	–	−12.63	–	Broken chamber[h]
VC	3A	81	85558		Bottom	−11.90	–	−25.54	–	–
VC	8B	44	n85450		Center	−3.49	–	−7.01	–	–
VC	10A	62	n85444		Center	−12.08	–	−25.74	–	–
MX	1B-1	1	85490		West end	−1.49	–	−15.48	–	From infilled bc
MX	14A-1	17	n85461		East end	−1.51	–	−9.66	–	Near apt, 14A-1
MX	8A-1	40	n85450		Center	−1.44	–	−13.38	–	Near mold, 8A-1
MX	10A-1	47	n85444		Center	−1.33	–	−13.42	–	Near venter, 10A-1
MX	16-5	7	85473		Top	−1.36	–	−13.11	–	MX in bite mark
MX	5B-1	66	n85484		Low center	−1.39	–	−13.40	–	Near 5B-1
CR	1B	55	n85490		West end	−1.27	–	−17.44	–	Exposed surface crust
CR	14A	24	n85461		East end	−1.65	–	−17.95	–	As above
CR	3B	77	85560		Bottom	−1.21	–	−17.01	–	As above

OS outer shell, *CC* chamber calcite (from inside phragmocone), chambers intact except as noted in footnote h, *VC* vein carbonate, *MX* concretion matrix (carbonate), *CR* concretion outer crust (carbonate)

apt aperture; *bc* body chamber; *ch* chamber; *phrag lat* phragmocone, lateral region; *siph* siphuncle

[a] Indicates samples submitted as replicates to assess measurement consistency; samples with a number (and letter) followed by a dash and another number are from the outer shell or the chamber of the ammonite specimen indicated; others were not on or in an ammonite (but may have been near one, see also footnote c)

[b] Randomly assigned number for purposes of blind measurements, i.e., the laboratory doing the measurements did not know the source of the sample

[c] "*n*" before number indicates that the sample is derived from matrix or crust of a specimen without an AMNH number, but near the indicated AMNH specimen

[d] PI = Preservation index as defined by Cochran et al. (2010)

[e] Location within the concretion

[f] Mean values calculated for duplicate analyses; these were the values used for analyses and plotting (Fig. 11) in the case of duplicate samples, otherwise the original sample value was used

[g] (Sample 41) from venter of body chamber adapical of the point of recurvature, close enough to sample 36 and from the same region of the ammonite to be considered as a duplicate

[h] Sample from a broken phragmocone chamber that was open to an open space in the adjoining body chamber that was not completely filled with matrix; all other chamber samples were from intact phragmocone chambers that were bored into by the investigators to obtain samples from inside

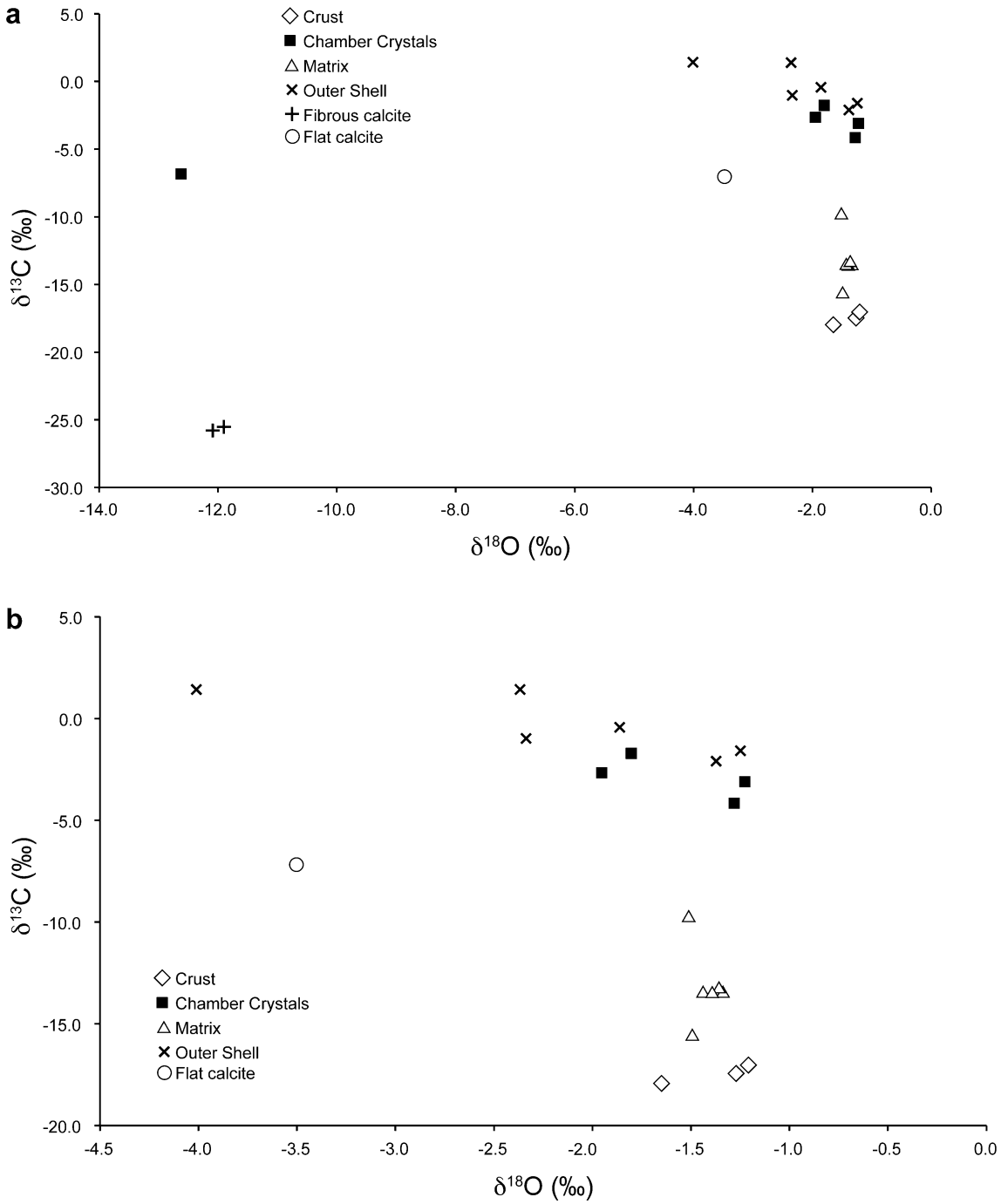

Fig. 11 Isotopic analysis of samples from the concretion. **a** All samples. **b** All samples excluding the fibrous calcite and one of the samples of chamber calcite

organisms such as scavenging gastropods may have been attracted to the area to feed on the stranded ammonite carcasses. Thus, the sequence of events involved the death and delivery of scaphites to the bottom, followed by the accumulation of intercepted, passing debris, coincident with the development of a community attracted to the site because of the high concentration of organic matter.

Acknowledgments We thank S. Thurston (AMNH) for photography and preparation of the figures, K. Sarg (AMNH) for scanning electron microscopy, G. Cane (KPESIL) for isotopic analyses, B. Saini-Eidukat (NDSU) for discussions about the interpretation of the isotopes, N. Larson (Larson Paleontology) for help and advice in preparing the sculpture, T. Linn (Glendive, MT) for help in the field, D. Schwert and A. Ashworth (NDSU) for first introducing JCG and JWG to the Cedar Creek Anticline and discussing the subject of this paper and related topics, L. Tackett (NDSU) for reviewing an earlier

draft of this manuscript, K. Grier for field assistance, D. Arneson (Hawley, MN) for help building the 3-D measuring frame and sculpture mount, B. Hussaini and M. Conway (AMNH) for administrative and curatorial assistance, K. D. Gomez (NDSU) for statistical advice, and the Cedar Creek Grazing Association (Glendive, MT) for permission to collect concretions on their land. This research was supported by the Norman D. Newell Fund (AMNH) plus personal funds (JCG and JWG).

References

Bamburak, J.D., & Nicolas, M.P.B. (2009). Revisions to the Cretaceous stratigraphic nomenclature of southwest Manitoba (parts of NTS 62F, G, H, J, K, N, O, 63C, F); in Report of Activities 2009, Manitoba Innovation, Energy and Mines, Manitoba Geological Survey, 183–192.

Baron-Szabo, R. (2008). Corals of the KT-boundary: Scleractinian corals of the suborders Dendrophylliina, Caryophylliina, Fungiina, Microsolenina, and Stylinina. *Zootaxa, 1952*, 1–244.

Berner, R.A. (1968). Calcium carbonate concretions formed by the decomposition of organic matter. *Science*, *159*, 195–197.

Bishop, G.A. (1967). Biostratigraphic mapping in the upper Pierre Shale utilizing the cephalopod genus *Baculites*, Cedar Creek Anticline, Montana: Unpublished M.S. thesis, Rapid City, South Dakota School of Mines and Technology, p. 1–18.

Bishop, G.A. (1973). Geology, stratigraphy, and biostratigraphy of the north end of the Cedar Creek Anticline, Dawson County, Montana. Montana Bureau of Mines and Geology Special Publication 61 (one page stratigraphic chart).

Canfield, D.E., & Raiswell, R. (1991). Carbonate precipitation and dissolution: Its relevance to fossil preservation. In P. A. Allison, D.E.G. Briggs (Eds.), *Taphonomy: Releasing the Data Locked in the Fossil Record* (pp. 411–453). New York: Plenum Press.

Carpenter, S. J., Erickson, J. M., Lohmann, K. C., & Owen, M. R. (1988). Diagenesis of fossiliferous concretions from the Upper Cretaceous Fox Hills Formation, North Dakota. *Journal of Sedimentary Petrology 58*(4), 706–723.

Clement, J.H. (1986). Cedar Creek: A significant paleotectonic feature of the Williston Basin: Part II. Northern Rocky Mountains. In J. A. Peterson (Ed.), *Paleotectonics and sedimentation in the Rocky Mountain Region, United States* (pp. 213–240). Tulsa, Oklahoma: American Association of Petroleum Geologists.

Cobban, W.A. (1969). The Late Cretaceous ammonites *Scaphites leei* Reeside and *Scaphites hippocrepis* (DeKay) in the Western Interior of the United States: U.S. Geological Survey Professional Paper 619, p. 1–29.

Cobban, W. A., Walaszczyk, I., Obradovich, J. D., & McKinney, K. C. (2006). A USGS zonal table for the Upper Cretaceous middle Cenomanian-Maastrichtian of the Western Interior of the United States based on ammonites, inoceramids, and radiometric ages. *United States Geological Survey. Open-File Report, 2006–1250*, 1–46.

Cochran, J. K., Kallenberg, K., Landman, N. H., Harries, P. J., Weinreb, D., Turekian, K. K., et al. (2010). Effect of diagenesis on the Sr, O, and C isotopic composition of Late Cretaceous mollusks from the Western Interior of North America. *American Journal of Science, 310*, 69–88.

Conrad, T.A. (1858). Observations on a group of Cretaceous fossil shells found in Tippah County, Miss., with descriptions of fifty-six new species. J*ournal of the Academy of Natural Sciences of Philadelphia*, ser. 2, 3, 323–336, pls. 34, 35.

Coryell, H. N., & Salmon, E. S. (1934). A molluscan faunule from the Pierre Formation in eastern Montana. *American Museum Novitates, 746*, 1–18.

Cossmann, M. (1904). Essais de paléoconchologie comparée. Paris, Presses Universitaire de France, 6, p. 1–261.

Dale, A., John, C. M., Mozley, P. S., Smalley, P. C., & Muggeridge, A. H. (2014). Time capsule concretions: unlocking burial diagenetic processes in the Mancos Shale using carbonate clumped isotopes. *Earth and Planetary Science Letters*, *394*, 30–37.

Davis, R. A., Landman, N. H., Dommergues, J.-L., Marchand, D., & Bucher, H. (1996). Mature modifications and dimorphism in ammonoid cephalopods. In N. H. Landman, K. Tanabe, & R. A. Davis (Eds.), *Ammonoid Paleobiology* (pp. 463–539). New York and London: Plenum Press.

Dennis, K. J., Cochran, J. K., Landman, N. H., & Schrag, D. P. (2013). The climate of the Late Cretaceous: New insights from the application of the carbonate clumped isotope thermometer to Western Interior Seaway macrofossils. *Earth and Planetary Science Letters, 362*, 51–65.

Elias, M. K. (1933). Cephalopods of the Pierre Formation of Wallace County, Kansas, and adjacent area. *University of Kansas Science Bulletin, 21*(9), 289–363.

Evans, J., & Shumard, B. F. (1854). Descriptions of new fossil species from the Cretaceous formation of Sage Creek, Nebraska, collected by the North Pacific Railroad Expedition, under Gov. J.J. Stevens. *Proceedings of the Academy of Natural Sciences of Philadelphia, 7*, 163–164.

Evans, J., & Shumard, B.F. (1857). On some new species of fossils from Cretaceous formations of Nebraska Territory. *Transactions of the Academy of Natural Sciences of Saint Louis*, *1*, 38–42.

Gill, J.R., & Cobban, W.A. (1966). The Red Bird section of the Upper Cretaceous Pierre Shale of Wyoming. *U.S. Geological Survey Professional Paper*, *393-A*, 1–73.

Grier, J. C., & Grier, J. W. (1998). New findings of the ammonite *Rhaeboceras*, including a new species, from the Pierre Shale of eastern Montana. *Journal of Paleontology, 72*, 473–476.

Grier, J. W., Grier, J. C., Larson, N. L., & Petersen, J. G. (2007). Synonymy of the ammonite genus *Ponteixites* Warren with *Rhaeboceras* Meek. *Rocky Mountain Geology, 42*, 123–136.

Grier, J. C., Grier, J. W., & Petersen, J. G. (1992). Occurrence of the upper Cretaceous ammonite *Rhaeboceras* in the *Baculites eliasi* zone of the Pierre Shale. *Journal of Paleontology, 66*, 521–523.

Grossman, E. L., & Ku, T. L. (1986). Oxygen and carbon isotope fractionation in biogenic aragonite: temperature effects. *Chemical Geology, 59*, 59–74.

Hall, J., & Meek F.B. (1856). Description of new species of fossils, from the Cretaceous formations of Nebraska, with observations upon *Baculites ovatus* and *B. compressus*, and the progressive development of the septa in *Baculites*, *Ammonites*, and *Scaphites*. *Memoirs of the American Academy of Arts and Sciences New Series*, *5*, 379–411.

Kauffman, E. G., & Caldwell, W. G. E. (1993). The Western Interior Basin in space and time. In W. G. E. Caldwell, E. G. Kauffman (Eds.), Evolution of the Western Interior Basin. Geological Association of Canada Special Paper, *39*, 1–30.

Kruta, I., Landman, N. H., & Cochran, J. K. (2014). A new approach for the determination of ammonite and nautilid habitats. *PLoS ONE, 9*(1), e87479.

Landman, N.H., & Cobban, W.A. (2007). Ammonite touch marks in Upper Cretaceous (Cenomanian-Santonian) deposits of the Western Interior Seaway. In N.H. Landman, R.A. Davis, R.H. Mapes (Eds.), *Cephalopods present and past: new insights and fresh perspectives* (pp. 396–422). New York: Springer.

Landman, N.H., Cobban, W.A., & Larson, N.L. (2012). Mode of life and habitat of scaphitid ammonites. *Science Direct/Geobios*, *45*, 87–98.

Landman, N. H., Cochran, J. K., Rye, D. M., Tanabe, K., & Arnold, J. M. (1994). Early life history of *Nautilus*: Evidence from isotopic analyses of aquarium-reared specimens. *Paleobiology, 20*, 40–51.

Landman, N. H., Kennedy, W. J., Cobban, W. A., & Larson, N. L. (2010). Scaphites of the *nodosus* group from the Upper Cretaceous (Campanian) of the Western Interior of North America. *American Museum of Natural History Bulletin, 342*, 1–242.

Landman, N. H., & Klofak, S. M. (2012). Anatomy of a concretion: life, death, and burial in the Western Interior Seaway. *Palaios, 27*, 671–692.

Larson, N.L., Jorgensen, S.D., Farrar, R.A., & Larson, P.L. (1997). *Ammonites and the other cephalopods of the Pierre Seaway* (p. 1–148). Tucson, Arizona: Geoscience Press.

Li, R. Y., Young, H. R., & Zhan, R. B. (2011). Drilling predation on scaphopods and other molluscs from the Upper Cretaceous of Manitoba. *Palaeoworld, 20*(4), 296–307.

Maeda, H. (1987). Taphonomy of ammonites from the Cretaceous Yezo Group in the Tappu area, northwestern Hokkaido, Japan. *Transaction and Proceedings of the Palaeontological Society of Japan, New Series, 148*, 285–305.

Maeda, H., & Seilacher, A. (1996). Ammonoid taphonomy, In N.H. Landman, K. Tanabe, R. A. Davis (Eds.), *Ammonoid Paleobiology* (pp. 543–578). New York and London: Plenum Press.

Martin, J.E., & Parris, D.C. (Eds.) (2007). The geology and paleontology of the Late Cretaceous marine deposits of the Dakotas. Geological Society of America Special Papers, p. 1–256.

Meek, F. B. (1872). Preliminary list of the fossils collected by Dr. Hayden's exploring expedition of 1871, in Utah and Wyoming Territories, with descriptions of a few new species. United States Geological and Geographic Survey of the Territorities. Preliminary Report, 5th. *Annual Report, 1871*, 373–377.

Meek, F.B. (1876). A report on the invertebrate Cretaceous and Tertiary fossils of the upper Missouri country. *United States Geological Survey of the Territories Report*, *9*, 1–629, pls. 1–45.

Meek, F.B., & Hayden, F.V. (1856a). Descriptions of twenty-eight new species of Acephala and one Gasteropod, from the Cretaceous formations of Nebraska Territory. *Proceedings of the Academy of Natural Sciences of Philadelphia 8*, 81–87.

Meek, F.B., & Hayden, F.V. (1856b). Descriptions of new species of Mollusca collected by Dr. F.V. Hayden, in Nebraska Territory; together with a complete catalogue of all the remains of Invertebrata hitherto described and identified from the Cretaceous and Tertiary formations of that region. *Proceedings of the Academy of Natural Sciences of Philadelphia*, *8*, 265–286.

Meek, F.B., & Hayden, F.V. (1860). Systematic catalogue, with synonyma, etc., of Jurassic, Cretaceous and Tertiary fossils collected in Nebraska, by the exploring expeditions under the command of Lieut. G.K. Warren, of U.S. Topograghical Engineers. *Proceedings of the Academy of Natural Sciences of Philadelphia*, *12*, 417–432.

Meek, F.B., & Hayden, F.V. (1861) Descriptions of new Lower Silurian, (Primordial), Jurassic, Cretaceous, and Tertiary fossils, collected in Nebraska, by the exploring expedition under the command of Capt. Wm F. Reynolds, U.S. Top. Engineers, with some remarks on the rocks from which they were obtained. *Academy of Natural Sciences of Philadelphia Proceedings*, *13*, 415–447.

Morton, S.G. (1842). Description of some new species of organic remains of the Cretaceous group of the United States: With a tabular view of the fossils hitherto discovered in this formation: *Journal of the Academy of Natural Sciences of Philadelphia, 8* (2), 207–227.

Olivero, E.B. (2007). Taphonomy of ammonites from the Santonian-lower Campanian Santa Marta Formation, Antarctica: Sedimentological controls on vertically embedded ammonites, *Palaios*, *22*, 586–597.

Owen, D.D. (1852). Report of a geological survey of Wisconsin, Iowa, and Minnesota; and incidentally of a portion of Nebraska Territory made under instructions from the United States Treasury Department (2 vols., pp. 1–638). Philadelphia: Lippincott, Grambo.

Palamarczuk, S., & Landman, N.H. (2011). Dinoflagellate cysts from the upper Campanian Pierre Shale and Bearpaw Shale of the U. S. Western Interior. *Rocky Mountain Geology*, *46*(2), 137–164.

Reboulet, S., & Rard, A. (2008). Double alignments of ammonoid aptychi from the Lower Cretaceous of Southeast France: Result of a post-mortem transport or bromalites? *Acta Palaeontologica Polonica, 53*(2), 261–274.

Reiskind, J. (1975). Marine concretionary faunas of the uppermost Bearpaw Shale (Maestrichtian) in eastern Montana and southwestern Saskatchewan. *Geological Association of Canada Special Paper*, *13*, 235–252.

Sageman, B.S., & Arthur, M.A. (1994). Early Turonian paleogeographic/paleobathymetric map, Western Interior, U. S., In M. Caputo, J.A. Peterson, & K.J. Franczyk, (Eds.), *Mesozoic Systems of the Rocky Mountain Region, U.S. Rocky Mountain Section, SEPM (Society for Sedimentary Geology) Special Publication*, 457–470.

Shackleton, N. J., & Kennett, J. P. (1975). Paleotemperature history of the Cenozoic and initiation of Antarctic glaciation: oxygen and carbon isotope analyses in DSDP sites 277, 279 and 281. *Initial Reports of the Deep Sea Drilling Program, 29*, 743–755.

Sohl, N.F. (1964). Neogastropoda, Opisthobranchia and Basommatrophora from the Ripley, Owl Creek, and Prairie Bluff Formations, Late Cretaceous gastropods in Tennessee and Mississippi. *Geological Survey Professional Paper*, *331-B*, 153–330.

Speden, I.G. (1970). The Type Fox Hills Formation, Cretaceous (Maestrichtian) South Dakota. Pt. 2. Systematics of the Bivalvia. Peabody Museum of Natural History Bulletin, *33*, p. 1–222.

Stephen, D. A., Bylund, K. G., Garcia, P., McShinsky, R. D., & Carter, H. J. (2012). Taphonomy of dense concentrations of juvenile ammonoids in the Upper Cretaceous Mancos Shale, east-central Utah. *USA Science Direct/Geobios, 45*, 121–128.

Takeda, Y., Tanabe, K., Sasaki, T., & Landman, N.H. (2015). Durophagous predation on scaphitid ammonoids in the Late Cretaceous Western Interior Seaway of North America. Lethaia DOI: 10: 1111/let.12130.

Tsujita, C.J. (1995). Origin of concretion-hosted shell clusters in the Late Cretaceous Bearpaw Formation, southern Alberta. *Palaios*, *10*, 408–423.

Tsujita, C.J., & Westermann, G.E.G. (1998). Ammonoid habitats and habits in the Western Interior Seaway: A case study from the Upper Cretaceous Bearpaw Shale of southern Alberta, Canada. *Palaeogeography, Palaeoclimatology, Palaeoecology*, *144*, 135–160.

Waage, K. M. (1964). Origin of repeated fossiliferous concretion layers in the Fox Hills Formation. *Kansas Geological Survey Bulletin, 169*, 541–563.

Walaszczyk, I., Cobban, W. A., & Harries, P. J. (2001). Inoceramids and inoceramid biostratigraphy of the Campanian and Maastrichtian of the United States Western Interior Basin. *Geneve, Revue Paleobiologie, 20*, 117–234.

Westermann, G. E. G. (1996). Ammonoid life and habitat. In N. H. Landman, K. Tanabe, & R. A. Davis (Eds.), *Ammonoid Paleobiology* (pp. 607–707). New York and London: Plenum Press.

Whitfield, R.P. (1877). Preliminary report on the palaeontology of the Black Hills. United States Geological and Geographic Survey of the Rocky Mountain Region (Powell), 1–49.

Wilson, D. D., & Brett, C. E. (2013). Concretions as sources of exceptional preservation, and decay as a source of concretions: Examples from the Middle Devonian of New York. *Palaios, 28*, 305–316.